THERMAL ANALYSIS OF AIR-COOLED FUEL CELLS

By

Setareh Shahsavari
M. Sc., Sharif University of Technology, 2009
B. Sc., Sharif University of Technology, 2006

THESIS SUBMITTED IN PARTIAL FULFILLMENT OF
THE REQUIREMENTS FOR THE DEGREE OF

MASTER OF APPLIED SCIENCE

In the
School of Engineering Science
Faculty of Applied Sciences

SIMON FRASER UNIVERSITY

Summer 2011

APPROVAL

Name: **Setareh Shahsavari**

Degree: **Master of Applied Science**

Title of Thesis: **Thermal Analysis of Air-cooled Fuel Cells**

Examining Committee:

Chair: **Dr. Siamak Arzanpour**

Assistant Professor of Engineering Science

_____

Dr. Majid Bahrami
Supervisor
Assistant Professor of Engineering Science

_____

Dr. Erik Kjeang
Supervisor
Assistant Professor of Engineering Science

_____

Dr. Farid Golnaraghi
Internal Examiner
Professor and Associate Director Engineering Science (Surrey); Burnaby Mountain Chair

Date Defended/Approved: _____

ABSTRACT

Temperature distribution in a fuel cell significantly affects the performance and efficiency of the fuel cell system. Particularly, in low temperature fuel cells, improvement of the system requires proper thermal management, which indicates the need for developing accurate thermal models. In this study, a 3D numerical thermal model is presented to analyze the heat transfer and predict the temperature distribution in air-cooled proton exchange membrane fuel cells (PEMFC). In the modeled fuel cell stack, forced air flow supplies oxidant as well as cooling. Conservation equations of mass, momentum, and energy are solved in the oxidant channel, while energy equation is solved in the entire domain, including the gas diffusion layers and separator plates, which play a significant role in heat transfer. Parametric studies are performed to investigate the effects of various properties and operating conditions on the maximum cell temperature. The present results are further validated with experiment. This model provides a theoretical foundation for thermal analysis of air-cooled PEMFC stacks, where temperature non-uniformity is high and thermal management and stack cooling is a significant challenge.

Keywords: PEM fuel cell; Air cooling; Thermal management; Forced convection; Heat transfer; Numerical modeling

ACKNOWLEDGEMENTS

I would like to thank my supervisors, Dr. Majid Bahrami and Dr. Erik Kjeang, for their excellent support during my graduate studies. Their professional attitude and positive personality have continually inspired me, and their encouragements have refreshed me in desperate moments. I would also like to thank Dr. Farid Golnaraghi for kindly reviewing this thesis.

I greatly appreciate the technical supports of Mr. Andrew Desouza from Ballard Power Systems. This project was financially supported by Natural Sciences and Engineering Research Council of Canada, NSERC and Ballard Power Systems.

TABLE OF CONTENTS

LIST OF FIGURES

LIST OF TABLES

NOMENCLATURE

A_c	cross-sectional area of the channel (m^2)
c	concentration (mol m^{-3})
c_p	specific heat (J K^{-1} kg^{-1})
D	diffusion coefficient (m^2 s^{-1})
E	maximum voltage obtained from converting enthalpy of formation of hydrogen into electrical energy (V)
F	Faraday's constant (C mol^{-1})
G	Gibbs free energy (J)
g	gravity acceleration (m s^{-2})
Gr	Grashof number
H	enthalpy (J)
h	convective heat transfer coefficient (W $m^{-2}K^{-1}$)
I	electrical current (Amp)
i	current density (Amp m^{-2})
k	thermal conductivity ($Wm^{-1}K^{-1}$)
l	length (m)
$\dot{m}$	mass flow rate (kgs^{-1})
N	molar flux (mol m^{-3})
n	outward unit normal
Nu	Nusselt number
P	pressure, (Pa)
Pr	Prandtl number
PEM	polymer electrolyte membrane fuel cell
$\dot{q}$	heat generation per unit volume (Wm^{-3})
$\dot{Q}$	total heat generation (W)
Ra	Rayleigh number
S	entropy (J K^{-1})
T	temperature (K)
t	thickness (m)
U_0	thermodynamic equilibrium potential of the reaction (V)
u	velocity (m s^{-1})
u	velocity vector (m s^{-1})
V	output voltage (V)
$\dot{W}$	power (W)
w	width (m), water vapour mass fraction

Greek symbols

β	volumetric thermal expansion coefficient (K^{-1})
μ	fluid viscosity ($N.s.m^{-2}$)
ν	kinematic viscosity ($m^2\ s^{-1}$)
ρ	density ($kg\ m^{-3}$)
ϕ	relative humidity
ω	humidity ratio

Subscript

BP	bipolar plate
CCM	catalyst coated membrane
cell	single fuel cell
ch	channel
cond	conduction
conv	convection
domain	domain
exp	experiment
f	fluid
GDL	gas diffusion layer
in	inlet, in-plane
irrev	irreversible
m	mean
max	maximum
MEA	membrane electrode assembly
out	outlet
rev	reversible
rib	rib
s	solid
sat	saturation
sim	simulation
thr	through-plane

1: INTRODUCTION

Fuel cells are devices that produce electricity through electrochemical reactions. In a proton exchange membrane fuel cell (PEMFC), a membrane separates oxidation and reduction half reactions. Figure **1-1** schematically shows the basic construction of a PEMFC. The fuel is hydrogen gas and the oxidant is ambient air or pure oxygen. The only byproducts of this reaction are heat and water. Considering their high energy conversion efficiency, zero emission potential, low noise and potential use of renewable fuels, fuel cells are considered as future devices for mobile, stationary, and portable power applications. However, PEMFC systems are not currently cost effective; increasing their efficiency for transportation and stationary applications can improve their commercialization [1].

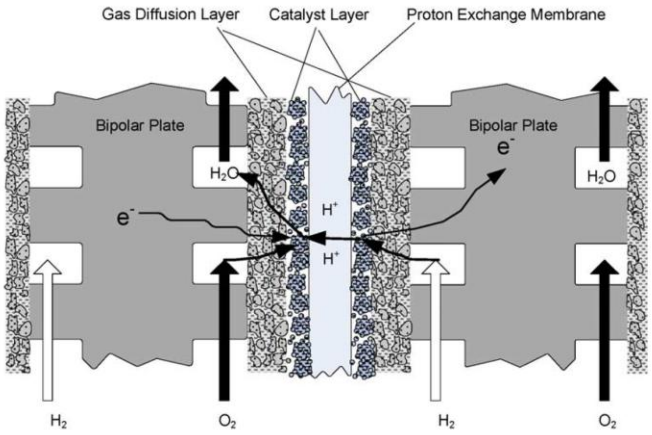

Figure 1-1: Basic construction of a typical PEM fuel cell [2].

Operation of a PEMFC is a complex process and includes transport of mass, momentum, energy, species and charges that take place simultaneously. Different parts of

a PEMFC are comprised of current collectors, anode and cathode flow channels, gas diffusion layers (GDLs), catalyst layers and the membrane. During the operation of a PEMFC, hydrogen molecules are supplied at the anode and split into protons and electrons. The polymeric membrane conducts protons to the cathode while the electrons are pushed round an external circuit and a current is generated from anode side to cathode side via electric load. Oxygen (form air) is consumed in the cathode side and reacts with the hydrogen ions, producing water and heat.

Fuel cells are still undergoing intense development, and the combination of new and optimized materials, improved product development, novel architectures, more efficient transport processes, and design optimization and integration are expected to lead to major gains in performance, efficiency, reliability, manufacturability and cost-effectiveness.

1.1 Influence of Temperature on Fuel Cell Performance

A simple way to improve the performance of a fuel cell is to operate the system at its maximum allowed temperature. At higher temperature, electrochemical activities increase and reaction takes place at a higher rate, which in turn increases the efficiency. On the other hand, operating temperature affects the maximum theoretical voltage at which a fuel cell can operate. Higher temperature corresponds to lower theoretical maximum voltage and lower theoretical efficiency [2].

Temperature in the cell also influences cell humidity, which significantly influences membrane ionic conductivity. Therefore, temperature has an indirect influence on the cell output power through its impact on the membrane water content. The

maximum operating temperature should be less than 100°C when a PEMFC operates at low pressure.

On the other hand, the durability of the membrane electrolyte is another barrier for higher-temperature operation due to performance degradation during long-term operation. In particular, PEMFCs employing perfluorosulfonic acid polymers (Nafion®) as a membrane electrolyte have the glass transition temperature ranging from 80 to 120°C, which leads to a serious break down of the MEA [3]. Furthermore, Endoh et al. [4] reported that the perfluorosulfonic acid polymer suffers from degradation under low-humidity operations even at 80°C. Therefore, the durability of the Nafion® membrane is another factor that limits the maximum operating temperature as 80°C.

As a result, the operating temperature is selected by considering the durability of the membrane electrolyte and the safety margin for thermal transient response of the fuel cell. The main purpose of thermal management in fuel cell systems is to ensure the stack operation within a reliable temperature range and to provide a more uniform temperature distribution in the stack. A detailed understanding of the stack thermal behaviour is therefore necessary for design and development of an efficient cooling solution. Oosterkamp [5] addressed some of the heat transfer issues for both PEM based systems and SOFC systems. To analyze the effectiveness of different thermal management strategies, developing a thermal model is essential. In the following section, a comprehensive literature review on PEMFC thermal models is presented.

1.2 Review of PEMFC Thermal Models

Several studies are available on analytical and numerical modeling of PEMFCs. However, a few of them have concentrated on the area of thermal modeling and thermal management. Fuel cell thermal models can be categorized as cell-level, stack-level, and system-level models based on the boundaries of the studied domain. Depending on the level of study, analytical or numerical approach can be adopted.

1.2.1 Analytical Models: System-level

Due to the complexity of PEMFC systems, system-level models do not include temperature gradient within the fuel cell stack. Most of the system-level thermal management studies in the literature are either experimental or simplified analytical models that consider isothermal condition for the fuel cell stack.

Xue et al. [6] presented a zero-dimensional (lumped) dynamic model to investigate the mixed effects of temperature, gas flow, and capacitance, with an emphasis on system transient behaviour. In their thermal model, only the convective heat transfer to the surrounding was considered. Another transient lumped model was developed by Yu and Jung [7]. They evaluated the control algorithms of cooling module for the thermal management of a PEMFC.

Bao et al. [8] developed a system-level model to analyze the effect of air stoichiometric ratio and the cathode outlet pressure on thermal loads of different components of a fuel cell system, including fuel cell stack, radiator, condenser, and, membrane humidifier.

In [9] by Yu et al., a simple analytical model was developed to investigate the performance of a Ballard water-cooled PEMFC stack. Using a set of gas feeding conditions (i.e., pressure, temperature, flow rate) and stack physical conditions (i.e., channel geometry, heat transfer coefficients, operating current) as input parameters, the model could provide information regarding the reaction products (i.e., water and heat), stack power, stack temperature, and system efficiency [9]. They considered a uniform stack temperature assuming a high thermal conductivity. However, this assumption cannot be justified for large-scale stacks or air-cooled fuel cells. Although the study of Yu et al. [9] was based on a specific Ballard PEM fuel cell, the results were not validated with experimental data.

Another system-level thermal management study was presented by Colella in [10], where different cooling loop configurations for a 6 kW combined heat and power fuel cell system were investigated to find the one with optimal heat recovery performance. These configurations were analyzed by applying the technique of Pinch Point Analysis, which minimizes the energy requirements for a process plant, to the fuel cell system [11]. In the model of [10], particular focus was on the position of condenser.

Chupin et al. [12] presented a pseudo two-dimensional performance model and included a one-dimensional thermal model for cooling water. Shan and Choe [13] also considered a one-dimensional temperature gradient across the fuel cell stack in the through plane direction; they assumed that the temperature is constant at each cell but varies from cell to cell.

1.2.2 CFD-based Models

There also exist several computational fluid dynamics (CFD) models of PEMFCs. A literature overview of models, ranging from one-dimensional, single-component to complete three-dimensional, large-scale setups, was presented by Siegel in [14] with an emphasis on heat and mass transfer. His review included modeling strategies and commonly used assumptions, solver implementations, popular numerical algorithms, and computational techniques. In addition, an overview of commonly used simulation software for fuel cell modeling was given in [14].

Among the CFD-based models that considered heat transfer, Yu and Jung [15] developed a two-dimensional numerical thermal model of a PEMFC and investigated a thermal management system for fuel cells with large active cell areas. Their fuel cell model was composed of sub-models for the water transport through the membrane electrolyte, the electrochemical reaction in the cathode catalyst layer and the temperature distribution within the fuel cell. Their heat transfer sub-model was focused on heat rejection from the fuel cell into the cooling water and included the conduction heat transfer inside the MEA and convective heat rejection from MEA to cooling water flow and gases. The thermal management system model of [15] included radiator, cooling pump and fan for investigating the trade-off between the temperature distribution effect and parasitic losses.

Pharoah and Burheim [16] presented a two-dimensional thermal model and obtained temperature distributions in a PEMFC in the plane normal to the cathode flow direction. In their work, only conductive heat transfer was considered. A three-dimensional model was developed by Shimpalee and Dutta [17], which solved the energy

equation to predict the temperature distribution inside a straight channel PEMFC. They analyzed the effect of heat produced by the electrochemical reactions on the fuel cell performance.

Adzakpa et al. [18] developed a three-dimensional dynamic model of a single cell to explain phenomena such as the cell humidity and voltage degradations. Their heat transfer model included the conduction and heat generation inside the fuel cell and the convection on the outer surface. Convective heat transfer inside the fuel cell was not considered in the model of [18]. A comprehensive three-dimensional model that included analysis of species, heat, and charge transport in a single-channel unit cell, was presented by Sinha and Wang [19]. They investigated the performance of a PEMFC operating at high temperature. In their thermal model, a constant temperature condition was applied on all the external boundaries of the fuel cell.

Ju et al. [20] presented a three-dimensional, thermal model coupled with electrochemical and mass transport models in order to study thermal and water management in PEMFCs. Their numerical simulation shows that the thermal effect on PEMFC becomes more critical at higher current density and/or lower gas diffusion layer thermal conductivity.

In the next section, various stack cooling methods with relevant studies in the open literature are introduced.

1.3 Stack Cooling Methods: Overview

There are different cooling methods that can be used in fuel cell systems to maintain a constant temperature. These include heat spreaders, cooling with cathode air flow, cooling with separate air flow, water cooling, and cooling with antifreeze/coolant [2].

1.3.1 Passive Methods

Passive cooling refers to design features used for cooling without power consumption.

- **Heat spreaders**

Employing heat spreaders with high thermal conductivity in a PEMFC stack is a passive cooling method. By using heat spreaders, heat can be transferred more efficiently outside the stack. Heat spreaders can be used to transport heat out of the stack through conduction, then to dissipate the heat to surrounding air through natural or forced convection. To add as little extra weight and volume as possible to the stack, high performance heat spreaders must be used.

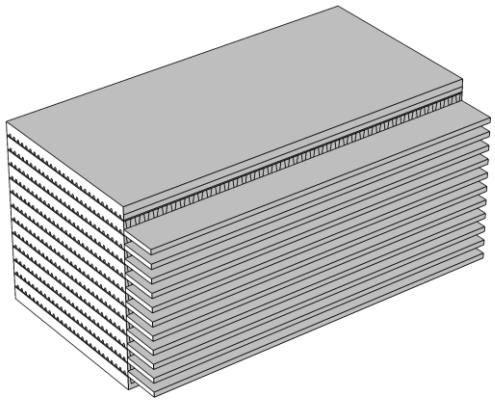

Figure 1-2: Schematic of a stack with heat spreaders/fins.

- **Heat pipes**

A heat pipe is essentially a passive heat transfer device that combines the principles of thermal conductivity and phase change and has an extremely high effective thermal conductivity. Faghri and Guo [21] studied recent applications of heat pipe technology in fuel cell systems, which include new stack designs with heat pipes to improve heat transfer as well as work on fuel cell system level design. In their study, in one design, a bipolar plate was designed with holes, into which micro-heat pipes were inserted and bonded (see Figure 1-3). In another design proposed in [21], flat heat pipes were integrated with a carbon bipolar plate for improving thermal control in the fuel cell stack.

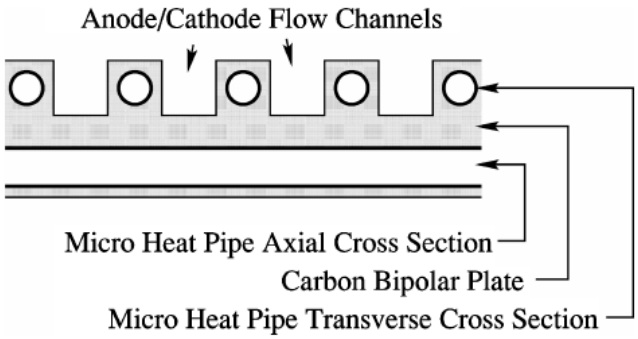

Figure 1-3: Micro-heat pipe embedded in a bipolar plate [21].

- **Natural cooling with cathode air flow**

For a small fuel cell, the cathode air flow can work in one of two modes: natural convection or forced convection. Natural convection is the simplest way to cool the cell zand evaporate water at the cathode. This is done with a fairly open structure at the cathode sides, which will increase the volume of the stack. For small PEM fuel cells (less

than 100W), natural convection from air breathing can be sufficient to maintain the cell temperature.

1.3.2 Active Methods

- **Forced cooling with cathode air flow**

Forced convection airflow is another convenient way to bring the waste heat out of the stack. This will result in a more compact stack structure and increase the cooling capability. However, very high cathode air flow velocity or a very large gas channel is necessary for removal of waste heat. When the power of the fuel cell is high, a more effective cooling approach must be applied. Essentially, air cooling method is simpler and needs fewer accessories compared to liquid cooling methods but as the output power increases, it becomes harder to maintain a uniform temperature distribution within the stack by air cooling method and the parasitic losses associated with the cooling fan increase inevitably.

Since the specific heat of air is low, high air flow rate is needed to remove the generated heat. In addition, the dimensions of air cooling channels should be larger than those of water cooling channels, which make the stack larger than what it needs to be. On the other hand, temperature distribution within the stack could be more uniform and the heat removal would be more efficient by using water cooling method; however, this method needs more accessories and complicated control schemes.

There are not many studies available in the area of air-cooled fuel cells. Sasmito et al. [22] developed a two-dimensional numerical model to study the forced-air convection heat transfer in an open-cathode PEMFC. They considered two-phase flow

and solved conservation equations of mass, momentum, species and energy in a single cell, which represented a fuel cell stack by applying periodic boundary conditions. It was demonstrated in [22] how the fan power and pressure drop over the cathode flow-fields in the stack affect the overall performance. Also the local distributions of the dependent field variables such pressure, temperature, velocity, and concentration were presented in [22].

The main applications of the air-cooled fuel cell is in portable and backup power generation, where fuel cell solutions have many advantages over conventional lead-acid batteries and diesel generators, including extended runtime, high reliability, high efficiency, and reduced environmental impact.

- **Cooling with separate air flow**

Although simply increasing reactant air flow can remove more heat, too much reactant air may dry out the proton exchange membrane [1]. In such cases, fuel cells will generally need a separate reactant air supply and cooling system.

Figure 1-4 illustrates a PEM fuel cell structure with separate cooling plates, through which air is blown. The advantage of this structure is that it can extract more heat from the stack without affecting the cathode air flow. Air-cooled designs using a bipolar plate integrated coolant flow are known for low temperature PEMFC [18, 23]. Different design concepts for an internally or externally cooled high temperature PEMFC (HT-PEMFC) have been presented in Ref. [24].

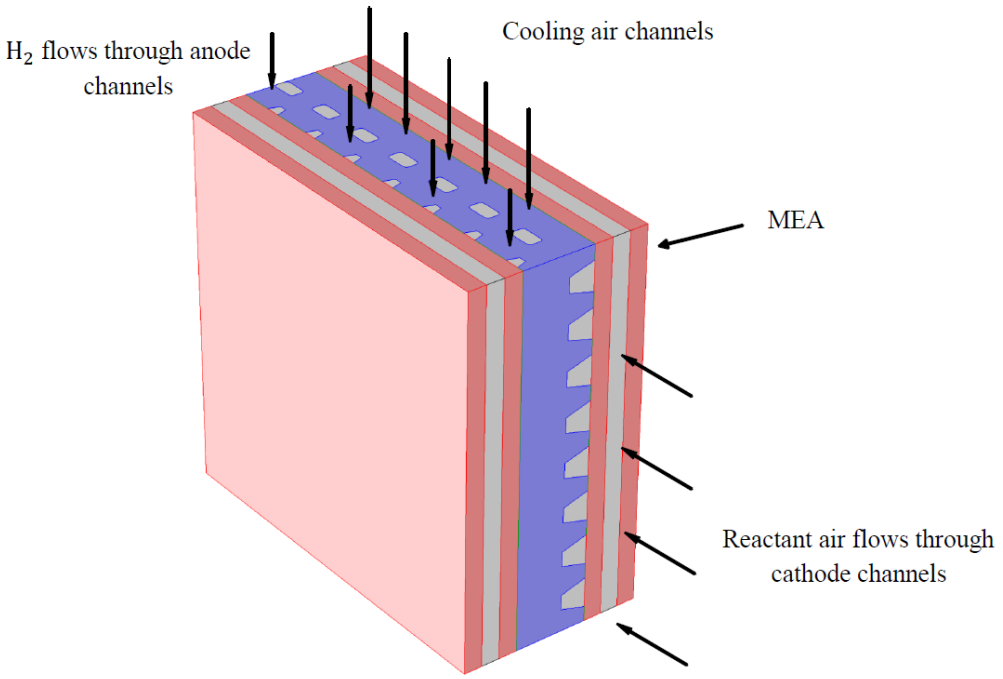

Figure 1-4 Schematic of two MEAs and one bipolar plate modified for separate reactant and cooling air in a PEM fuel cell

- **Water cooling**

For hydrogen PEMFCs larger than 10 kW, it is generally necessary to use water cooling. Units below 2 kW can be air cooled, and cells between 2 kW and 10 kW need a careful choice regarding whether air or water cooling should be used [1]. Water cooling requires a more complex design: the temperature and pressure of the cooling water must be monitored and the flow of cooling water must be supplied by a water pump. Stack cooling in direct methanol fuel cells (DMFCs) is relatively simpler, since increasing circulation of dilute methanol solution at the anode could remove more waste heat from the stack. The water cooling of PEMFCs gives rise to problems associated with water management such as preventing the product water from freezing, and rapidly melting any frozen water during start-up when the fuel cell system is operated in sub-freezing

conditions. In such situations, an antifreeze/ coolant is used instead of normal water in the cooling system.

Most of the PEMFC thermal management studies in the literature are focused on water-cooling. Asghari et al. [25] designed a thermal management subsystem for a water-cooled 5kW PEMFC system and numerically studied the cooling flow field performance. In the CFD based thermal model of [25], experimental polarization curve was used as the input parameter to calculate the amount of heat generation at different working voltage. The number of parallel channels in parallel serpentine flow field was selected as the design parameter of the flow field and its optimum value was obtained by compromising between the minimum pressure drop of coolant across the flow field and maximum temperature uniformity within the bipolar plate criteria.

Baek et al. [26] numerically investigated fluid flow and heat transfer in cooling plates of a water-cooled PEMFC and assessed the performance of different coolant flow field designs in terms of the maximum temperature, temperature uniformity, and pressure drop characteristics. According to [26], multi-pass serpentine flow field designs could significantly improve the uniformity of temperature distribution in a cooling plate compared with the conventional serpentine flow field designs, while a similar maintaining the coolant pressure drop. The model of [26] only considers the cooling plate and does not provide temperature distribution inside the stack.

Kurina et al. [27] addressed the heat transfer performance of various cooling channel designs including parallel, serpentine, wavy, and, coiled. In their study, the cooling channel was designed to be placed on top of an electronic chip, which dissipates

heat at a constant flux. The results can be used for thermal management of PEMFC and battery stacks as well.

Song et al. [28] designed a stack cooling system for a high-temperature (above 100°C) water-cooled PEMFC. They implemented a pumpless cooling concept using the phase-change latent heat of water to decrease the parasitic power required for operating the system. This concept was based on the buoyancy force caused by the density difference between vapour and liquid when operated above boiling temperate, which was utilized to circulate the coolant between the stack and the cooling device.

1.3.3 Experimental Studies

Park and Caton [29] experimentally investigated the effect of air relative humidity on performance and temperature of a PEMFC stack and showed that fully hydrated inlet gases play a positive role both for water transport and to maintain the fuel cell stack temperature to prevent stack drying.

Wen et al. [30] experimentally investigated the effects of the pyrolytic graphite sheets on the performance and thermal management of a PEMFC stack. In their experiment, these graphite sheets were cut into the shape of flow channels and bounded to the cathode gas channel plates.

The features of pyrolytic graphite sheets are light weight and high thermal conductivity, which make it possible to use them as heat spreaders in the fuel cell stack to reduce the volume and weight of cooling systems and to homogenize the temperature in the reaction areas. It was shown in [30] that the maximum power of the stack can be increased more than 15% with pyrolytic graphite sheets attached.

Figure 1-5: Picture of the flow channel plate and the shaped pyrolytic graphite sheets [30].

In another study, Wen et al. [31] extended their work [30] and compared a stack with combined passive and active cooling with three other cooling configurations without passive cooling (pyrolytic graphite sheets) with different fan sizes. Although the maximum power generated by the stack with the configuration combining pyrolytic graphite sheets and fans was not the highest among all configurations, it reduced the volume, weight, and cooling power of the thermal management system [30].

1.4 Objectives

Regarding the crucial influence of temperature on PEMFC performance, thermal management is required to ensure stack operation within a reliable temperature range and to provide temperature uniformity in the stack. To analyze the effectiveness of different thermal management strategies, developing a thermal model is essential.

Accurately studying of heat transfer in a PEMFC requires consideration of the three-dimensional effects. However, the majority of the available numerical models are either not three-dimensional or are complex and involve high computational cost that makes it almost impossible to do parametric studies.

Our objective is to develop a three-dimensional thermal model of a PEMFC stack with reasonable computational cost, in order to predict temperature distribution and heat transfer coefficients and to analyze different thermal management strategies and do parametric studies. The focus is on air-cooled PEMFCs, in which forced convection heat transfer inside the stack plays an important role. Air-cooled fuel cell systems combines the cooling function with the cathode flow field and thus eliminates many of the auxiliary systems required for conventional fuel cell designs and by this mean lowers the overall cost.

The results of the present model are successfully validated by experimental data collected by Ballard Power Systems. In this study, the main goal is investigation of heat transfer in a PEMFC, in order to employ for developing new cooling strategies. Therefore, in chapter 3, parametric studies are performed to investigate the effects of air velocity and thermophysical parameters such as bipolar plate and gas diffusion layer (GDL) thermal conductivity on the stack temperature.

2: MODEL DEVELOPMENT

In this chapter, first, we introduce the transport phenomena in PEMFCs with governing equations that are solved in our model and the assumptions that were considered. Finally, we validate the results for temperature distribution with experiments.

2.1 Transport phenomena in PEMFCs

The cathode side of the MEA, shown schematically in Figure 1-1, provides a good illustration of the complex coupling between various transport phenomena in PEMFCs. The MEA consists of a proton exchange membrane sandwiched between catalyst and gas diffusion layers, with the latter two components essentially forming the electrode. This electrode is a buffer zone that facilitates a number of processes [32]:

- The conduction of electrons between the current collectors and the reaction sites.
- The conduction of protons between the membrane and catalyst layer.
- The transport of the reactants to the catalyst layer.
- The transport of heat away from the reaction site primarily through the solid matrix.
- Condensation/evaporation and transport of liquid water and vapour.

One of the most challenging aspects of computational modeling of PEMFCs is the multi-physics nature of the transport processes, and the coupling between these processes

as illustrated in Figure 2-1. Each circle in the figure represents a transport equation governing a particular process, and the arrows pointing outward represent the effects of a given transport process on other equations.

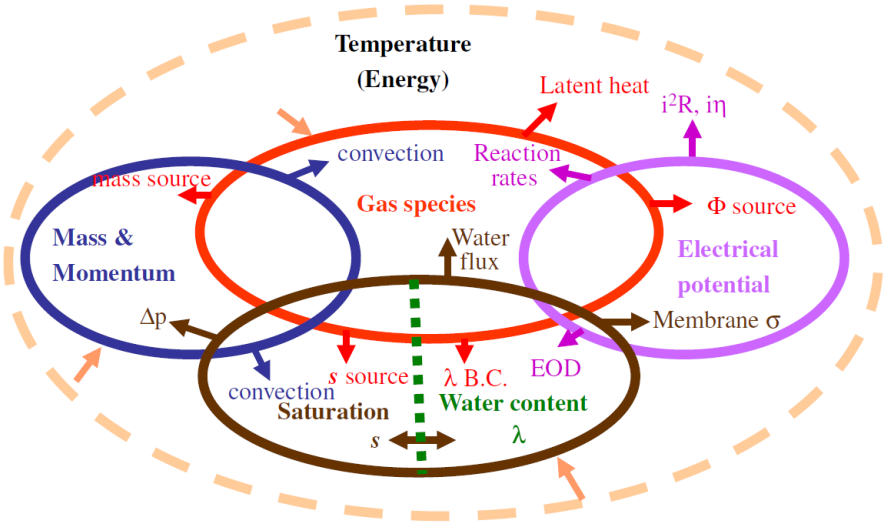

Figure 2-1: Coupling of Transport Phenomena in a PEMFC [32].

The development of a complete three-dimensional PEMFC model that considers all the components with simultaneous transport phenomena is a complex and challenging task. Furthermore, if the whole fuel cell stack composed of several cells is considered as the computational domain, modeling multi-physics processes involves significant computational cost, even by using high performance advanced numerical algorithms and taking advantage of parallel computing. One approach to overcome this problem is decoupling different processes by making simplifying assumptions that are reasonable and maintain the accuracy of the model. As an instance, when heat transport is the main interest of the analysis, we can skip solving equations of conservation of charge and species and instead, use the required input parameters from already existing models that capture other transport phenomena in a fuel cell, as it is done in this study.

2.2 Heat Transfer in a Fuel Cell Stack

Figure 2-2 shows the schematic of an air-cooled stack and a single channel and different modes of heat transfer. Heat transfer modes in a fuel cell stack include:

Natural convection from the outer surface of the stack to ambient air.

Forced convection in the channels and porous layers.

Conductive heat transfer in the solid phase, i.e. bipolar plates, GDLs, and catalyst coated membrane.

Radiation heat transfer from the stack surface.

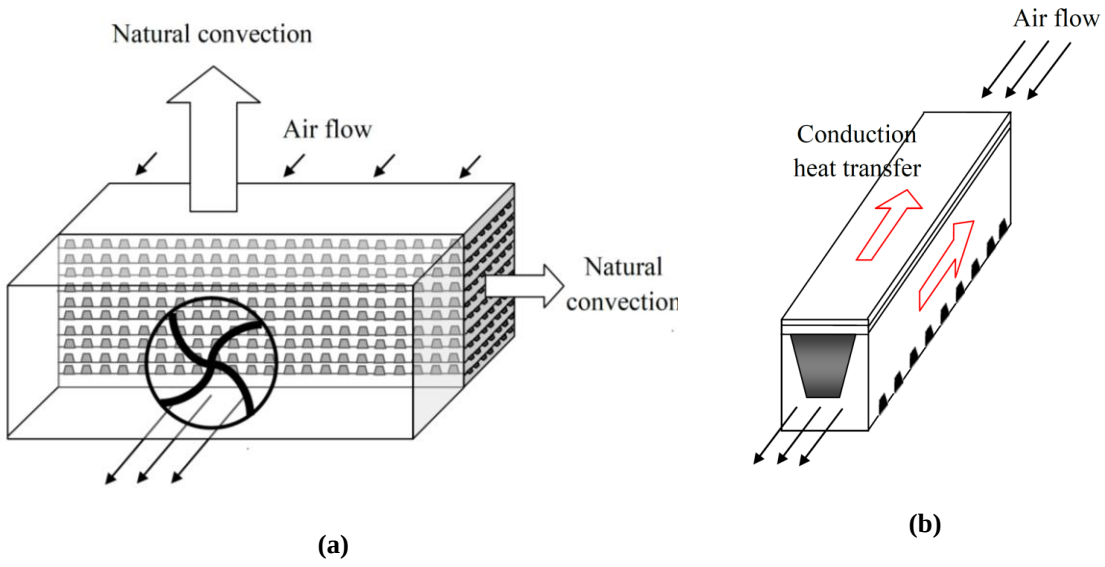

Figure 2-2 : Schematic of heat transfer (a) in an air-cooled stack and (b) in a single channel

As explained previously, it is desirable to operate the fuel cell system at a temperature slightly below the maximum allowable temperature. Therefore, predicting the maximum temperature in a stack is of high importance. Intuitively, one can predict that the maximum temperature occurs somewhere in the central cells of a fuel cell stack and the other cells that are closer to the outer surface experience a lower temperature as a

result of heat transfer from the outer surface. Similarly, in a single cell we expect that the temperature in the central channel will be higher than the other channels. Since one of the main interests of this research is to predict the maximum temperature in a stack, the complete stack is not modeled. Instead, we have considered the central cathode channel with plate and GDLs surrounding it in the central cell, which is expected to experience the maximum temperature in the entire stack. Taking advantage of symmetry in the fuel cell geometry, the computational domain is half of a single cathode channel as sketched in Figure 2-3.

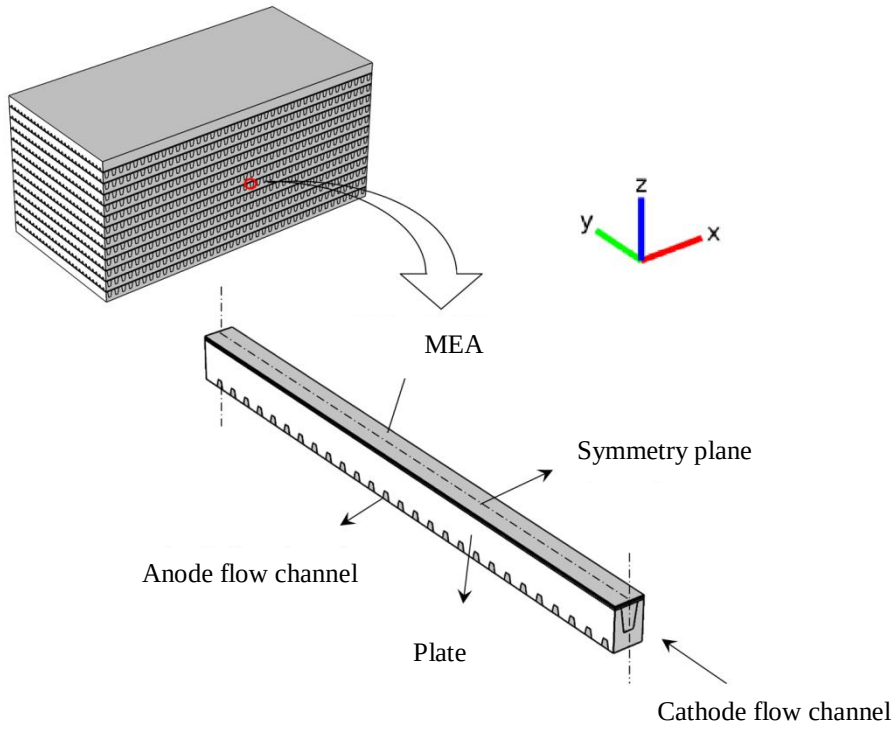

Figure 2-3 : 3D schematic of a fuel cell stack and a cathode channel, the computational domain

Since air-cooled stack is studied here, we should include the air domain before entering the cathode channel and after exiting the outlet. Otherwise, the heat transfer

from the end walls cannot be accurately captured in the model. Even considering an equivalent convective heat transfer coefficient does not lead to the same results as when including the air domain in the inlet and outlet. A schematic of the computational domain including inlet and outlet air is shown in Figure 2-4.

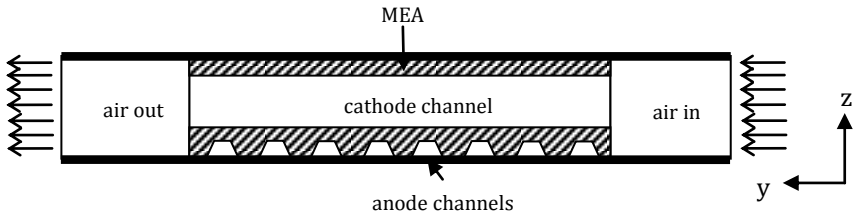

Figure 2-4: 2D schematic of the computational domain including ambient air before and after the channel; the dark lines on top and bottoms specify the periodic boundary condition.

In the present study, we have considered heat transfer in the entire domain and laminar fluid flow in the oxidant channel. The convective heat transfer in the hydrogen channels and porous gas diffusion layers is negligible due to the relatively low velocity of fluid in these regions. Also, considering the central channel as the computational domain, it can be shown that radiation heat transfer is negligible since the temperature is not high and also the surface area of the ends are small compared to the total surface area. The model inputs are current density, cell voltage, and inlet air temperature and velocity.

2.3 Governing Equations

In this section, the governing equations that are solved through our modeling process are described. Since the considered computational domain includes both solid and fluid sub-domains, the respective equations are presented separately.

2.3.1 Energy Equation

For the solid region, the mechanism of heat transfer is conduction. The energy equation is as follows:

$$\nabla.(k_s \nabla T_s) + \dot{q} = 0 \qquad \textbf{(2-1)}$$

where T_s is the temperature of the solid region. The term, $\dot{q}$, is the source term for heat generation and is assumed to be zero in all the domain except in the cathode catalyst layer, where the reaction heat is released. The following section describes how this term is calculated.

2.3.2 Heat Generation

The total heat release from a PEM fuel cell can be derived according to thermodynamics. In order to determine the amount of heat produced by a fuel cell, an energy balance for a fuel cell stack can be provided:

$$\sum_i H_{\mathrm{i,in}} = \sum_i H_{\mathrm{i,out}} + \dot{W}_{\mathrm{stack,gross}} + \dot{Q}_{\mathrm{total}} \qquad \textbf{(2-2)}$$

where $H_{\mathrm{i,in}}$ and $H_{\mathrm{i,out}}$ are the enthalpies of reactants and products respectively. The total heat generation, $\dot{Q}_{\mathrm{total}}$, is thus given by:

$$\dot{Q}_{\text{total}} = \dot{Q}_{\text{rev}} + \dot{Q}_{\text{irrev}} \quad \textbf{(2-3)}$$

Consider a H_2/O_2 fuel cell operated at temperature, T, pressure, P, and current, I. The reversible heat release, $\dot{Q}_{\text{rev}}$, can be written as:

$$\dot{Q}_{\text{rev}} = (-T\Delta S).\dot{N}_{H_2} = (-T\Delta S)\frac{I}{2F} = \left(-T\frac{\partial U_0}{\partial T}\right)I \quad \textbf{(2-4)}$$

where ΔS represents the entropy change of the overall reaction, $H_2 + \frac{1}{2}O_2 \rightarrow H_2O$, and U_0 the thermodynamic equilibrium potential of the reaction [33]. In addition, there exists irreversible heat generation due to the cell operated at a different voltage, V_{cell}, from the equilibrium, U_0. This additional heat generation rate is given by:

$$\dot{Q}_{\text{irrev}} = (-\frac{\Delta G}{2F} - V_{\text{cell}})I = (U_0 - V_{\text{cell}})I \quad \textbf{(2-5)}$$

where ΔG is the Gibbs free energy change of the H_2/O_2 reaction. This irreversible heat generation is attributed to ohmic and activation polarizations in a PEMFC. The total heat generation, $\dot{Q}_{\text{total}}$, is thus given by:

$$\begin{aligned}\dot{Q}_{\text{total}} &= \left(-T\frac{\partial U_0}{\partial T}\right)I + (U_0 - V_{\text{cell}})I \\ &= \left(U_0 - T\frac{\partial U_0}{\partial T}\right)I - V_{\text{cell}}\,I\end{aligned} \quad \textbf{(2-6)}$$

Notice that the first term on the right side of equation (2-6) is the maximum chemical power available from the overall reaction and the second term is the actual electrical power produced by a fuel cell. The energy efficiency can then be conveniently defined as the ratio of these two terms.

$$\eta_{\mathrm{e}} = \frac{V_{\mathrm{cell}}\, I}{\left(U_0 - T\frac{\partial U_0}{\partial T}\right) I} = \frac{V_{\mathrm{cell}}}{U_0 - T\frac{\partial U_0}{\partial T}} \qquad \textbf{(2-7)}$$

The heat calculated using equation (2-6) can be approximated by the following equation [12]:

$$\dot{Q}_{\mathrm{total}} = (E - V_{\mathrm{cell}}) I n_{\mathrm{cell}} \qquad \textbf{(2-8)}$$

where n_{cell} is the number of cells in a stack and E is the maximum voltage obtained if the hydrogen heating value or enthalpy of formation were transformed into electrical energy, and is given by [1]:

$$E = -\frac{\Delta H}{nF} \qquad \textbf{(2-9)}$$

The enthalpy of formation of water vapour at 25℃, 100 kPa is -241,826 kJ/kmol. Therefore, if the lower heating value (LHV) is used, E(25℃)=1.253 V. The cases in which water finally ends in liquid form are so few [1]. So we will restrict the analysis to the vapour case.

$E = 1.48\ V$ if using HHV

or $= 1.25\ V$ if using LHV

$\dot{Q}_{\mathrm{total}}$ must be transferred away from the cell to maintain a steady operating temperature for the fuel cell. It should be noted that by using the LHV, the cooling effect of evaporation is implicitly included in heat production of equation (2-8). It also means that energy is leaving the fuel cell in three forms: as electricity, as ordinary sensible heat, and as the latent heat of water vapour.

In this study, we use V_{cell} and I from experimental measurements. In future work, a performance model will be integrated with the current thermal model, from which V_{cell} and I can be calculated.

Due to symmetry, we have solved the equations in half of the domain. The symmetry boundary condition is applied on the side walls, which is equivalent to no heat flux in the normal direction across this boundary. Also periodic heat condition is applied on the top and bottom surfaces of the cell, where it contacts the adjacent cells in the stack. This boundary condition implies that $T(\text{at } z_{\min}) = T(\text{at } z_{\max})$ and also $\dot{q}_n(\text{at } z_{\min}) = \dot{q}_n(\text{at } z_{\max})$ (see axes in Figure 2-3).

2.3.3 Fluid Flow

For the fluid region, continuous, steady state, laminar (Re < 800), incompressible flow (Ma < 0.3) is assumed; therefore, the mass conservation, momentum principle, and energy equation are as follows

$$\nabla.(\rho\mathbf{u}) = 0 \qquad \textbf{(2-10)}$$

$$\rho\mathbf{u}\cdot\nabla\mathbf{u} = -\nabla p + \mu\nabla^2\mathbf{u} \qquad (2\text{-}11)$$

$$\rho c_p\mathbf{u}\,.\nabla T_f = \nabla.(k\nabla T_f) \qquad (2\text{-}12)$$

Since the flow is continuous, we have no slip and no temperature jump over the wall. Therefore, the boundary condition for velocity field is $u(\text{at wall}) = 0$ and for temperature field is T (at wall) $= T_{\text{wall}}$. The flow enters with a constant uniform velocity, u_{in}, and constant temperature, T_{in}. For the fluid flow conditions at the outlet, no viscous stress along with constant pressure are considered, as follows,

$$\left(\mu(\nabla \mathbf{u} + (\nabla \mathbf{u})^T) - \frac{2}{3}\mu(\nabla \mathbf{u})\mathrm{I}\right)\mathbf{n} = 0, \qquad \textbf{(2-13)}$$

$$p = p_{\mathrm{atm}}$$

where p_{atm} is the atmospheric pressure. This boundary condition is physically equivalent to the flow exiting into a large container. Note that because of the low velocity of hydrogen in the anode channels, we have neglected the convective heat transfer in anode side. Therefore, the only governing equation in anode channels is the same as equation (2-1). In addition, constant thermophysical properties have been assumed for solid phase while air properties such as density, heat capacity, dynamic viscosity, and thermal conductivity vary with temperature. Air density is obtained from ideal gas law.

2.3.4 Natural Convective Heat Transfer

It is expected that most of the generated heat in a fuel cell stack will be removed by the forced air flow; however, some smaller portions of the heat may be removed by free convection from stack faces to surrounding. To predict the maximum temperature in the stack, we neglected the effect of free convection and considered an insulated channel. However, to investigate the effect of heat removal by the free convection, we have solved other cases in which natural convective heat transfer from bipolar plate edges to surrounding is included in the numerical model. Heat convection coefficients are separately determined for vertical and horizontal edges by governing relations (2-14)-(2-17**)** from Incropera and DeWitt [34]:

$$h = \frac{Nu_l k}{l} \qquad \textbf{(2-14)}$$

$$\boldsymbol{Nu_l = 0.68 + \left[\frac{0.67Ra^{1/4}}{(1+(0.492/Pr)^{9/16})^{4/9}}\right]} \quad \textbf{(2-15)}$$

$$Ra = Gr\ Pr \quad (2\text{-}16)$$

$$Gr = \frac{g\beta(T_s - T_\infty)L^3}{\vartheta^2} \quad (2\text{-}17)$$

2.3.5 Transport of Species

In this section, we study the equations governing the transport of water vapour produced by the chemical reaction in cathode channel. The rate of water generation is derived by equation (2-18).

$$\dot{m}_{\mathrm{H_2O,produced}} = \frac{IM_{\mathrm{H_2O}}}{2F} \quad \textbf{(2-18)}$$

The transport of water vapour in the air stream takes place through convection and diffusion. We have used the Transport of Diluted Species interface in COMSOL Multiphysics 4.0a, which enables us to model the evolution of chemical species transported by diffusion and convection. This interface assumes that all present species are dilute, i.e. their concentration is small compared to a solvent fluid. As a rule of thumb, a mixture containing several species can be considered dilute when the molar concentration of the solvent is more than 90%. Due to the dilution, mixture properties such as density and viscosity can be assumed to correspond to those of the solvent.

When the diffusing species is dilute with respect to a solvent, Fick's law is adequate to describe the diffusive transport in the flux vector. As a result, the mass balance equation can be written in the form of equation (2-19).

$$\frac{\partial c}{\partial t} + \mathbf{u} \cdot (D\nabla c) = \nabla \cdot (D\nabla c) + R \quad \textbf{(2-19)}$$

where the dependent variable, c, is the concentration of the species (mol/m^3) , D denotes the diffusion coefficient (m^2/s), R is a reaction rate expression for the species (mol/m^3·s), and, **u** is the velocity vector (m/s) .

The first term on the left-hand side of equation (2-19) corresponds to the accumulation (or consumption) of the species. The second term accounts for the convective transport due to the velocity field, **u**. This field is obtained from coupling mass balance to momentum balance. On the right-hand side of the mass balance equation (equation (2-19)), the first term describes the diffusion transport, accounting for interaction between the dilute species and the solvent.

The diffusion coefficient of water vapour in air depends on temperature and can be described by the following relation proposed by Bolz and Tuve [35], plotted in

Figure 2-5.

$$D = -2.775 \times 10^{-6}\left[\frac{m^2}{s}\right] + 4.479 \times 10^{-8}\left[\frac{m^2}{s.K}\right]T + 1.656 \times 10^{-10}\left[\frac{m^2}{s.K^2}\right]T^2 \quad \textbf{(2-20)}$$

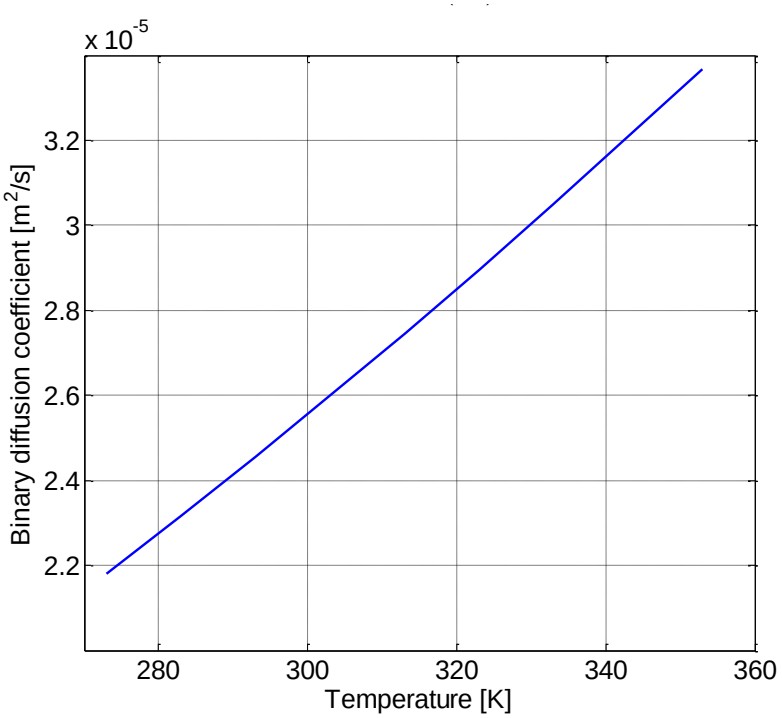

Figure 2-5: Diffusion coefficient of water vapour in air [35].

Finally, the second term on the right-hand side of equation (2-19) represents a source or sink term, typically due to a chemical reaction. In a PEMFC, water is produced through reaction in cathode catalyst layer. Since in our model, the computational domain for the mass conservation is the oxidant channel, we define the water vapour production as a mass/mol flux boundary condition at the interface of cathode GDL and oxidant channel to specify the total species flux across the boundary. This implies that we have assumed all the produced water goes to the oxidant channel. The total flux of species c is defined accordingly:

$$-\mathbf{n} \cdot (c\mathbf{u} - D\nabla c) = N_0 \qquad \textbf{(2-21)}$$

where N_0 is the molar flux expression (SI unit: mol/(m^2·s)) due to the chemical reactions.

$$N_0 = \frac{i}{2F} \tag{2-22}$$

At the inlet, air relative humidity is known. As such, the boundary condition at the inlet is constant concentration: $c = c_{\text{in}}$ (SI unit: mol/m^3). The inlet concentration is calculated using equations (2-23)-(2-26).

$$c_{\text{in}} = \frac{w_{\text{in}}\rho_{\text{in}}}{M_{\text{H}_2\text{O}}} \tag{2-23}$$

$$w_{\text{in}} = \frac{\omega_{\text{in}}}{1 + \omega_{\text{in}}} \tag{2-24}$$

$$\omega_{\text{in}} = 0.622\frac{P_{\text{v,in}}}{P_0 - P_{\text{v,in}}} \tag{2-25}$$

$$P_{\text{v,in}} = \phi_{\text{in}} P_{\text{sat,in}} \tag{2-26}$$

where w_{in}, ρ_{in}, ω_{in}, $P_{\text{v,in}}$, $P_{\text{sat,in}}$, and, ϕ_{in} are the inlet vapour mass fraction, air density, humidity ratio, vapour partial pressure, and saturated pressure respectively.

At the outlet, the species is transported out of the model domain by the fluid flow. In mass transport models where it can be assumed that convection is the dominating effect which causes the mass flow through the outflow boundary, the diffusive effect from this boundary can be ignored, such that:

$$\mathbf{n} \cdot (-D\nabla c) = 0 \tag{2-27}$$

This is a useful boundary condition, particularly, in convection-dominated mass balances where the outlet concentration is unknown.

We have used symmetry and periodic boundary conditions, similar to those for solving momentum and energy equations.

Table 2-1. Geometrical and thermophysical parameters used in the reference case.

t_{BP}	5.50 mm	$t_{\mathrm{rib,anode}}$	1.50 mm
$t_{\mathrm{GDL,anode}}$	0.20 mm	$k_{\mathrm{BP,thr}}$	20 W/m.K
$t_{\mathrm{GDL,cathode}}$	0.20 mm	$k_{\mathrm{BP,in}}$	60 W/m.K
t_{CCM}	0.05 mm	$k_{\mathrm{GDL,in}}$	10 W/m.K
l_{cell}	280.0 mm	$k_{\mathrm{GDL,thr}}$	0.7 W/m.K
w_{cell}	60.00 mm	k_{CCM}	1.5 W/m.K
$h_{\mathrm{ch,\ cathode}}$	2.50 mm	$k_{\mathrm{H_2}}$	0.18 W/m.K
$h_{\mathrm{ch,anode}}$	1.50 mm	D	From equation (2-20)
$w_{\mathrm{ch,\ cathode}}$	2.50 mm	V_{cell}	From experiment or performance model
$w_{\mathrm{ch,\ anode}}$	1.00 mm	I	From experiment or performance model
$t_{\mathrm{rib,cathode}}$	1.50 mm	E	1.253 V

The results of solving the equation of transport of species are presented in the next chapter. It should be noted that the inlet air relative humidity would affect the performance of a PEMFC. In the present model, we are using experimental values for current density and voltage. Therefore, the inlet relative humidity should be from the experiments as well. Parametric study to investigate the effect of air inlet relative humidity on the fuel cell temperature can be performed provided that the present model is coupled with a performance model. The thermophysical properties used in the reference case are listed in Table 2-1.

2.4 Summary of Assumptions

The following is a summary of the assumptions we made to model the fluid flow and heat transfer in an air-cooled PEMFC stack. Each of these assumptions is explained in the relevant sections.

- Continuous, steady state, laminar ($Re<800$), incompressible flow ($Ma<0.3$) was assumed.
- The central channel was considered to be insulated.
- Convective heat transfer in anode channel and GDL was neglected.
- Constant thermo-physical properties were assumed for the solid phase.
- Radiation heat transfer was neglected (based on scale analysis).
- Uniform heat generation in MEA was considered.
- LHV was used for heat generation.

2.5 Mesh Independency

The computational domain (see Figure 2-6) was created in COMSOL Multiphysics 4.0a. Three different amount of mesh elements- 3.5×10^5, 7.0×10^5 and 1.4×10^6- were implemented and compared in terms of local temperature, velocities, and pressure to ensure a mesh independent solution. We found that the mesh size of around 7.0×10^5 gives approximately 1% deviation compared to the mesh size of 1.4×10^6; whereas, the results from 7.0×10^5 mesh elements deviate up to 7% as compared to those from the finest one. Therefore, a mesh of around 7.0×10^5 elements was sufficient for the numerical investigation purposes: a fine structured mesh near the wall to resolve the

boundary layer and an increasingly coarser mesh in the middle of the channel in order to reduce the computational cost.

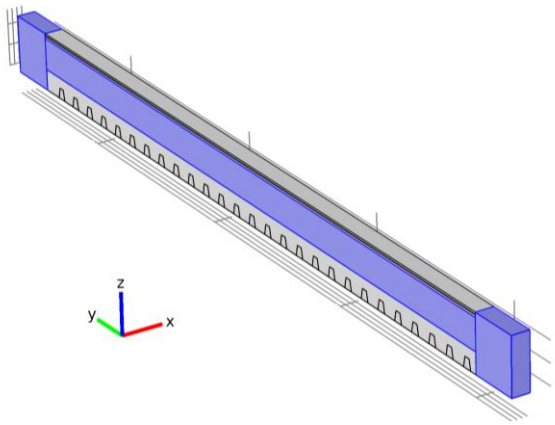

Figure 2-6: Computational domain for the PEMFC thermal model with inlet and outlet air domain.

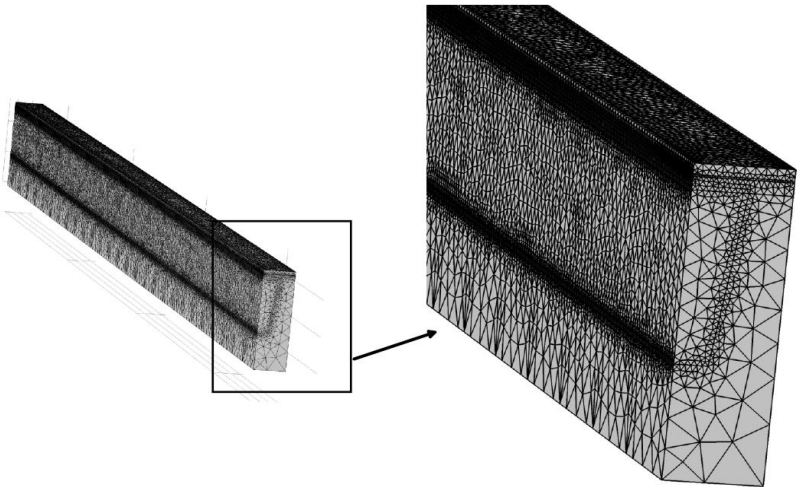

Figure 2-7: Mesh configuration of the computational domain with a single flow channel.

3: RESULTS AND DISCUSSION

For solving the system of partial differential equations explained in chapter 3, we have used COMSOL Multiphysics 4.0a. Grid independency was checked by solving a case study using different element size, which led to identical results. In our base/reference case (describe in Table 2-1), the inlet air velocity was selected 3.0 m/s, the inlet air temperature was 20℃, and the total heat generated in one cell, was 36W. Assuming 60 channels in one cell, the total heat generated in the domain (half channel) was 0.3W.

3.1 Base Case Results

Figure 3-1 shows the temperature contours in the middle cross section of the channel. A uniform temperature distribution in the solid region is observed, whereas relatively high temperature gradient exists in the flow channel. Also in Figure **3-2**, temperature contours are shown in different sections along the channel. For better description of temperature distribution in the solid and fluid regions, their temperature variations along x, y, and z directions are plotted in Figure 3-3 and Figure 3-4. The horizontal axis shows the normalized location: $x/x_{\max}, y/y_{\max}, z/z_{\max}$, where $x_{\max}$, $y_{\max}$, and $z_{\max}$, specify the boundaries of the domain in x, y, and z.

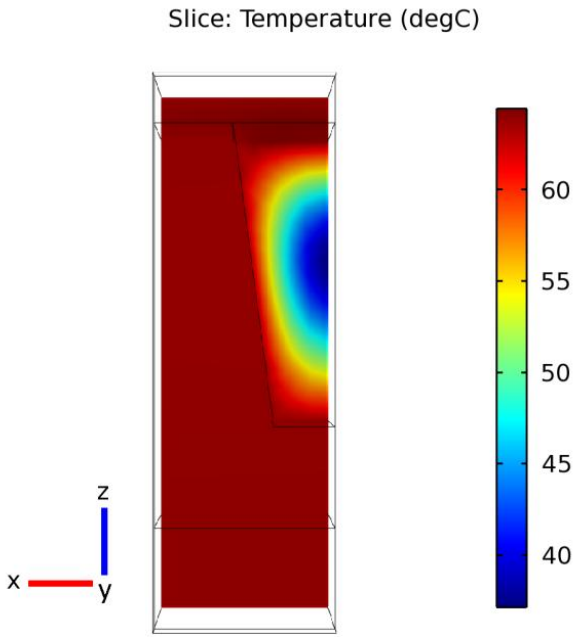

Figure 3-1: Temperature contours in the middle cross section of the channel (reference case).

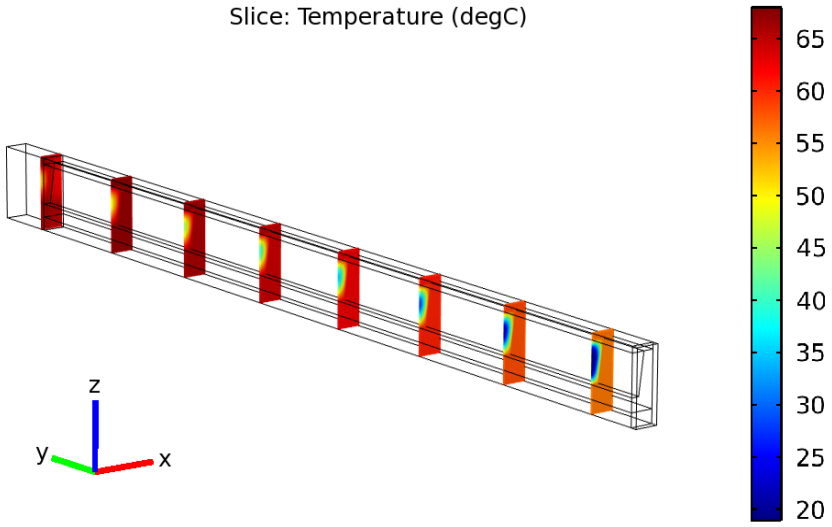

Figure 3-2: Temperature contours in eight slices from inlet to outlet of the channel (reference case).

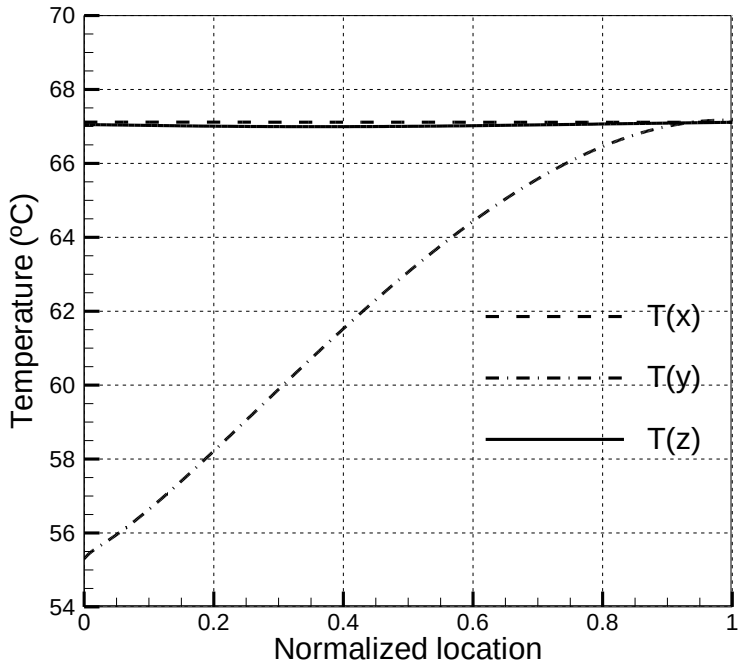

Figure 3-3: Temperature variation in different directions in bipolar plate (reference case).

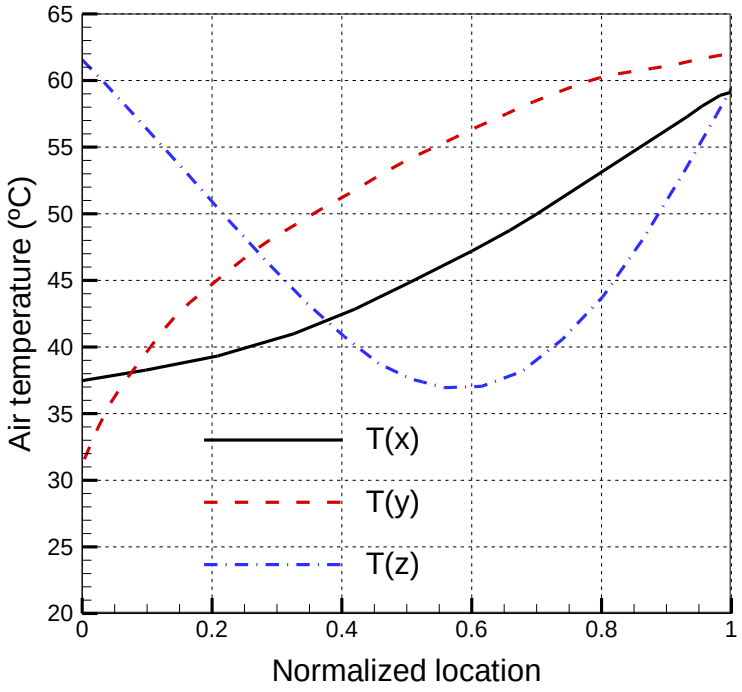

Figure 3-4: Temperature variation in different directions in air (reference case).

As previously mentioned, two major modes of heat transfer in this problem are forced convective heat transfer in cathode channels and conductive heat transfer in the

entire domain. The temperature gradient (which is mainly in y direction) determines the direction of convective and conductive heat flux, schematically shown in

Figure 3-5. The average value of these two heat fluxes at different cross-sections along the channel is calculated and plotted in Figure 3-6. As it can be inferred from this plot, the convective heat flux is two orders of magnitude higher than conductive heat flux. Moreover, the convective heat transfer almost remains constant along the channel, while in the same direction, conductive heat flux is decreasing. This is due to the different variation of the flow temperature gradient and the overall temperature gradient. In addition, conductive heat transfer is only changing by temperature gradient, which is decreasing; however, convective heat flux also depends on fluid density and velocity, which are not constant.

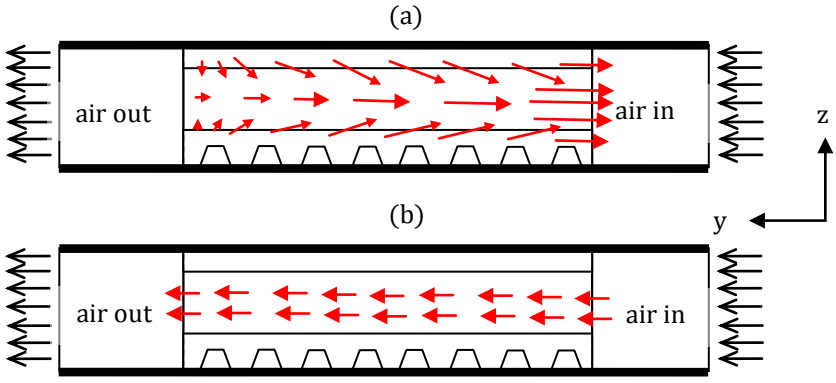

Figure 3-5: Schematic of heat flux vectors; (a) conductive heat flux, (b) convective heat flux

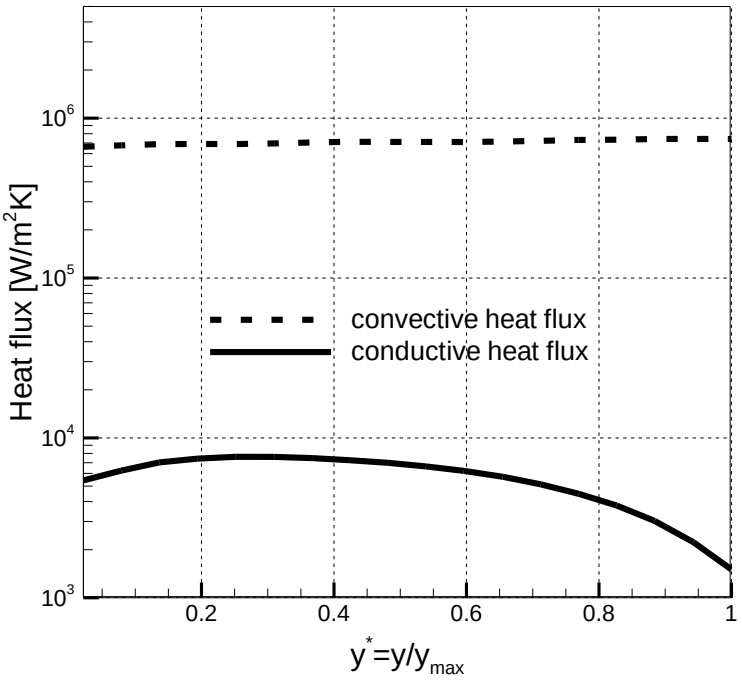

Figure 3-6: Absolute value of mean conductive and convective heat flux in the direction of air flow (reference case)

Table 3-1: Comparison of conductive and convective heat transfer. All parameters are kept constant in different cases except the oxidant flow rate and plate thermal conductivity

Case#	Air velocity $u_{in}[\mathrm{m/s}]$	Plate thermal conductivity $k_{\mathrm{BP}}[\mathrm{W/m.K}]$	Convective heat transfer $\dot{Q}_{\mathrm{conv}}[\mathrm{W}]$	Conductive heat transfer $\dot{Q}_{\mathrm{cond}}[\mathrm{W}]$	Percentage of convective heat transfer	Percentage of conductive heat transfer
1	4.0	30	0.289	0.011	96%	4%
2	3.0	50	0.27	0.03	90%	10%
3	2.0	30	0.264	0.036	88%	12%
4	4.0	60	0.262	0.038	87%	13%

In Table 3-1, the values of total convective and conductive heat transfer from the domain are calculated using the following relations,

$$\dot{Q}_{conv} = \dot{m}_{air} c_p (T_{m,out} - T_{m,in}) \quad \textbf{(3-1)}$$

$$\dot{Q}_{cond} = \left| \int_{A_{in}} k \frac{\partial T}{\partial y}\Big|_{y=0} dA \right| + \left| \int_{A_{out}} k \frac{\partial T}{\partial y}\Big|_{y=y_{max}} dA \right| \quad (3\text{-}2)$$

where, $T_{m,in}$ and $T_{m,out}$ are the air mean temperatures calculated from (3-3), at the inlet and outlet of the channel, respectively and A_{in} and A_{out} or the cross-sectional area of the solid walls in the inlet and outlet.

$$T_m = \frac{\int_{A_c} \rho u c_p T dA_c}{\dot{m}_{air} c_p} \quad \textbf{(3-3)}$$

Also, the percentage of each type of heat transfer, under different conditions (air velocity and plate thermal conductivity), are compared in Table 3-1. In higher air velocities, convection is the major part of heat transfer, and the contribution of conductive heat transfer becomes more important as the plate thermal conductivity increases.

For the reference case, we have also solved the equation of conservation of species. Adding the air relative humidity to our model does not affect the temperature distribution directly. Relative humidity has impact on the ionic conductivity of the membrane and by this means influences the output voltage and current. Therefore, as long as we provide experimental values for voltage and current we do not need to solve the equation of species transport to predict the temperature field. In order to see the direct impact of air relative humidity on temperature, a performance model should be integrated to the present thermal model.

Figure 3-7 and Figure 3-8 respectively, show water vapour mass fraction and relative humidity distribution in the cathode channel for the reference case. There is a mass flux from the top surface of the channel; consequently, the mass fraction of water vapour increases along the channel. In the studied case, the inlet relative humidity is 30% and the outlet is 11%. The local relative humidity has its maximum value (43%) approximately 1 cm from the cathode inlet.

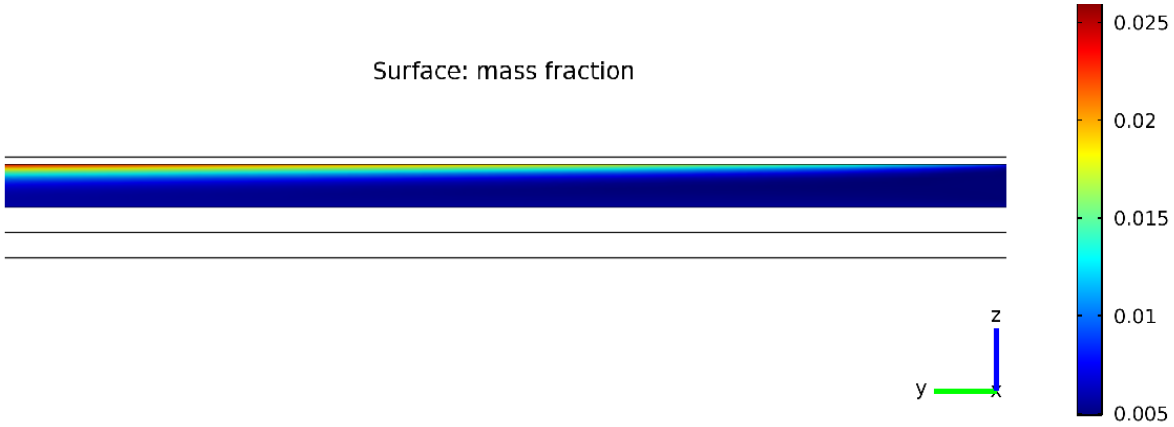

Figure 3-7: Water vapour mass fraction distribution in cathode channel

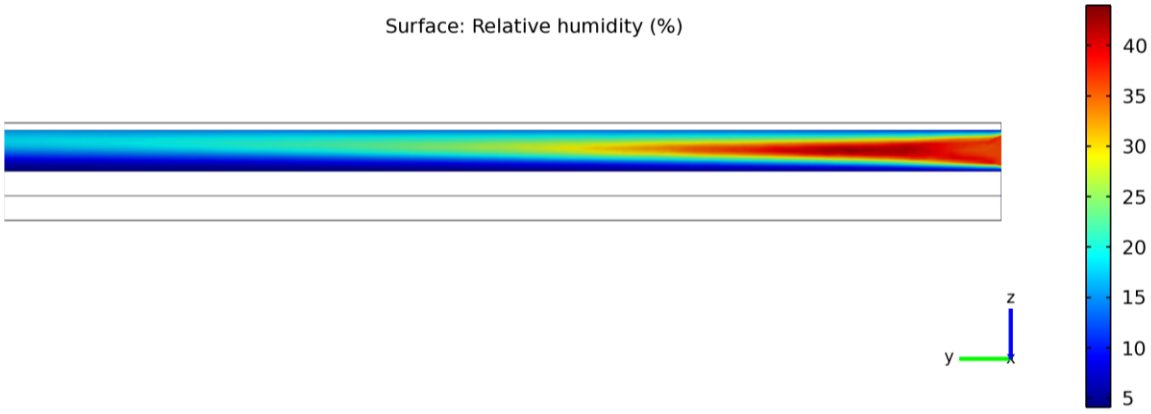

Figure 3-8: Relative humidity distribution in cathode channel

The variation of average value of relative humidity and water vapour mass fraction is plotted in Figure 3-9. Two factors affect the relative humidity: water vapour

accumulation and temperature. Although water vapour diffuses to the channel, it is noteworthy to observe that the average relative humidity is decreasing along the channel. This is due to the temperature rise in the air flow, which increases the saturation pressure and controls the relative humidity. The relative humidity is the ratio of vapour partial pressure to the saturation pressure at the same temperature:

$$\phi = \frac{P_{\mathrm{v}}}{P_{\mathrm{sat}}} \qquad \textbf{(3-4)}$$

In Figure 3-9, the horizontal axis starts from the inlet of the channel. Since the air temperature goes up slightly before entering the channel, relative humidity is less than $\phi_{\mathrm{in}} = 30\%$ at the cathode inlet.

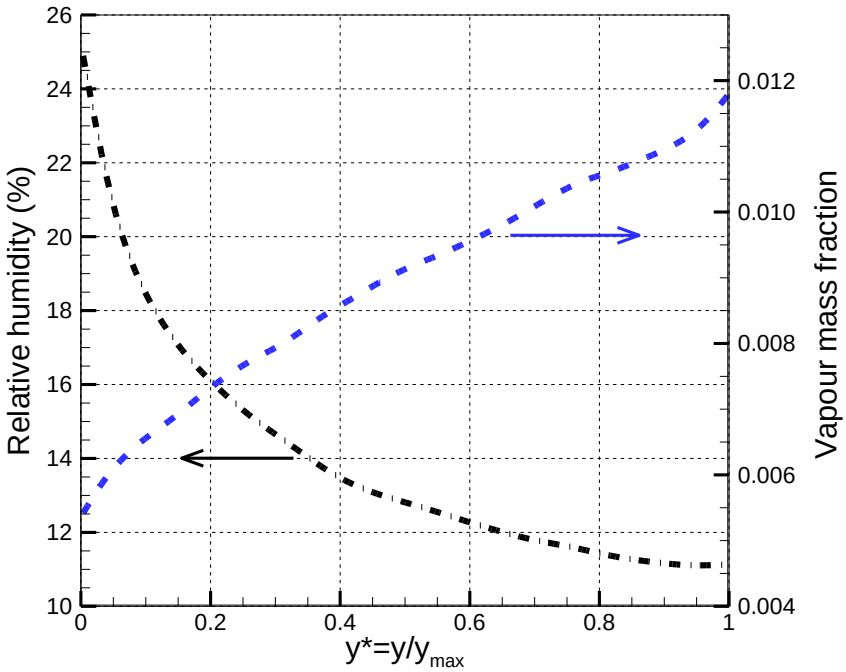

Figure 3-9: Relative humidity and vapour mass fraction along the cathode channel

3.2 Model Validation

3.2.1 Comparison with Experiments

For validating the present model, simulations under certain conditions have been performed and compared with the experimental data provided by Ballard Power Systems for an air-cooled fuel cell stack consisting of 28 cells. We have used the experimental operating conditions as input to our model. The temperature was measured using thermocouples located in different locations in the fuel cell stack. The maximum measured temperature was at the central cell of the stack as expected. In these experiments, the inlet air temperature was constant at room temperature while the air velocity and heat generation were varying in different cases. The amount of heat generation was calculated using experimental values of cell current and voltage in different operating conditions. The velocity was calculated using the fan volumetric flow rate and area. The results of our model validation are presented in Table 3-2, the last column of which shows the relative difference between predicted maximum temperature and experimentally measured maximum temperature. The location of the experimental temperature measurement is the outlet of the central channel in the middle row of the stack.

Table 3-2. Model validation.

Test #	Air inlet temperature [℃]	Air inlet velocity, $u_{\text{in}}[\text{m/s}]$	Heat generated in one cell, $\dot{Q}_{\text{cell}}$ [W]	Maximum temperature, $T_{\max}$ [℃]		Relative difference, $\frac{T_{\text{sim}}-T_{\text{exp}}}{T_{\text{sim}}}$
				Experiment*	Simulation	
1	21	2.19	37.7	65	68	4.4%
2	21	1.63	27.6	61	64	4.7%
3	21	1.45	29.1	67	69	2.8%
4	21	0.95	6.3	35	36	2.7%
5	21	0.94	13.7	50	54	7.4%

* Experimental results from Ballard Power Systems

3.2.2 Comparison with Analytical Model

In an earlier study [36], we have developed analytical solutions for velocity and temperature distributions of laminar fully developed flow of Newtonian, constant property fluids in channels of various cross-sections. The only limitation for the cross-section is that it should have at least two symmetry axes. Therefore, we are not able compare the numerical results of trapezoid channel with the analytical model of [36]. However, it is possible to compare the results of our numerical simulation with the analytical solution for square or rectangular cross-sections.

In the analytical model, hydrodynamic and thermal characteristics of the flow are derived. Two important characteristics of convective flow in channels are the Poiseuille number and the Nusselt number. The Poiseuille number, fRe, is the common dimensionless number used for analyzing pressure drop in channels and is defined by:

$$fRe = -\frac{1}{\mu}\frac{dp}{dy} \times \frac{D_h^2}{2u_m} \quad \textbf{(3-5)}$$

where D_h is the hydraulic diameter. The Nusselt number, Nu, is the ratio of convective to conductive heat transfer normal to the boundary and is defined by:

$$Nu = \frac{hD_h}{k} \quad \textbf{(3-6)}$$

Using equation (3-7), convective heat transfer coefficient, h, is calculated from the temperature distribution. In this equation, Γ is the cross-section perimeter, T_s is the wall temperature, which is constant at each cross-section, and T_b is the fluid bulk temperature.

$$h = \frac{\dot{m}c_p\frac{\partial T}{\partial y}}{\Gamma(T_s - T_b)} \quad \textbf{(3-7)}$$

We have modified our reference case geometry to model a cathode channel with square and rectangular cross-section keeping the cross-sectional area constant. The value of the Poiseuille calculated from the analytical and numerical models are compared in Table 3-3 for square and rectangular cross-section with aspect ratio of 0.5. Also Table 3-4 compares the Nusselt number obtained from numerical model and analytical models of [36] and [37] for isoflux and isotherm boundary conditions. As it can be seen in Table 3-3, the Poiseuille numbers derived from the two approaches are relatively close. The Nusselt number of the numerical model is higher than that of the analytical solution. The main reason is due to the different boundary conditions that were applied in the two

cases; in the analytical study, constant heat flux was uniformly applied on the channel walls while in the numerical model, the heat flux was applied only on the top wall of the channel.

Table 3-3: Comparison of Poiseuille number in rectangular channel derived from the analytical and numerical models.

Aspect ratio	fRe (Analytical, [36])	fRe (Numerical)	Relative difference
1	14.23	15.61	8%
0.5	15.55	16.95	8%

Table 3-4: Comparison of Nusselt number in rectangular channel derived from the analytical and numerical models.

Aspect ratio	Nu_{H1} (Analytical,[37])	Nu (Numerical)	Relative difference	Nu_{H2} (Analytical [36])	Nu (Numerical)	Relative difference
1	3.61	4.2	14%	3.09	4.2	26%
0.5	4.12	3.9	5%	3.02	3.9	22%

Using the new geometries, in addition to comparing the analytical and numerical results for pressure drop and heat transfer coefficient, we are able to investigate the effect of channel geometry on the fuel cell temperature. The results for geometrical parametric study are presented in chapter 4.

3.3 Natural Convection Effects

To investigate the effect of heat removal by the free convection, we have solved cases in which natural convective heat transfer from bipolar plate edges to surrounding is included in the numerical model. In Figure 3-10, the central and side channels are specified. We assumed symmetry boundary condition to solve the governing equations in the central channel. For the side channels, we consider natural heat transfer from one side and assume that other side is insulated. Thus, the symmetry boundary condition cannot be implemented and we have to consider the whole channel as the computational domain.

Figure 3-11 shows the bipolar plate temperature variation in the direction of flow for the central channel (thermally insulated) and side channel (with natural convection from one side) under the operating conditions of the base case. Temperature gradients are similar in both cases since the amount of heat generation and air flow rate are kept constant. The contribution of natural convection to the total heat transfer was 23% in this case as presented in Table 3-5.

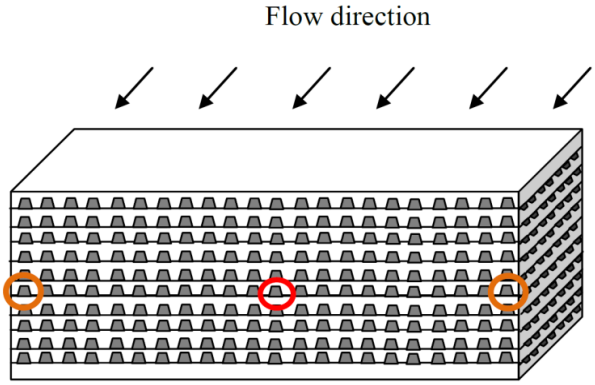

Figure 3-10: Schematic of the stack configuration. The specified channels in the stack can be covered by the present numerical model.

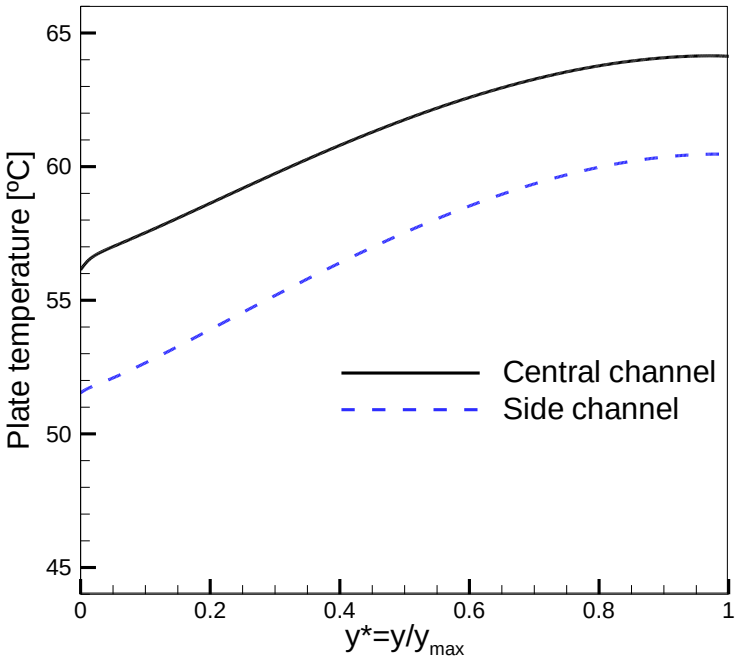

Figure 3-11: Bipolar plate temperature variation in the direction of flow for the central channel (thermally insulated) and side channel (with natural convection from one side)

Table 3-5: Comparison of heat transfer in central channel and side channel (base case).

Case	Total heat source	Natural convection	Forced convection	Conduction from inlet	Conduction from outlet
Insulated channel	0.6 W	-	0.510 W	0.083 W	0.007 W
	Percentage of total	-	85%	14%	1%
Side channel	0.6 W	0.140 W	0.387 W	0.068 W	0.005 W
	Percentage of total	23%	65%	11%	1%

The result of this model is also compared with experimental data for one test. Figure 3-12 (a) shows the schematic of one bipolar plate and Figure 3-12 (b) represents

the temperature distribution in the plate obtained from interpolation using 24 different temperature data measured by thermocouples in the central row of the stack. The experimental and numerical values for the plate temperature in the channel inlet and outlet are compared for the central and side channels.

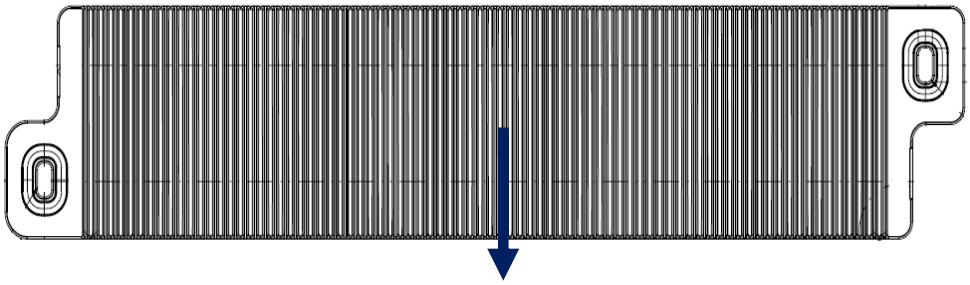

direction of air flow

(a)

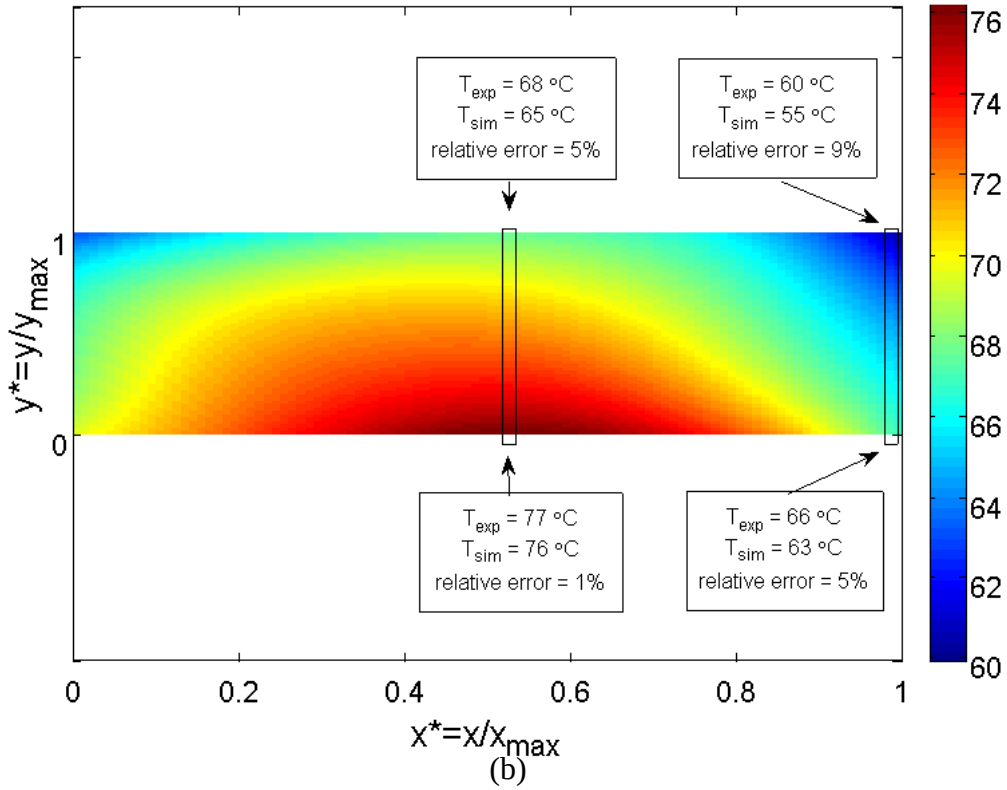

(b)

Figure 3-12: (a) Bipolar plate configuration, (b) Temperature distribution in one plate, interpolated using experimental data points. The experimental and numerical values for the inlet and outlet temperatures are compared for the central and side channels.

The relative errors in predicting the maximum and minimum temperature in the side channel are 5% and 9% respectively. In addition to the simplifying assumptions that were made in this model, the main sources of error can be: uncertainty in predicting natural convection heat transfer coefficient, non-uniformity in heat generation in one cell, and uncertainty in air velocity calculation. Regarding the latter, we have assumed equal air velocities for different channels, which might not be the real case.

4: PARAMETRIC STUDY

In this section, we investigate the effect of different parameters such as air inlet velocity, bipolar plate thermal conductivity, and GDL thermal conductivity on the maximum temperature and temperature distribution in the fuel cell stack. Regarding the thermal conductivities, we have considered isotropic and anisotropic material properties to study the impact of in-plane and through-plane thermal conductivity. In the parametric studies, only one parameter is varied while all other inputs parameters are kept the same as the reference case (see Table 2-1).

4.1 Thermal Properties and Operating Conditions

In air-cooled fuel cells, convective heat transfer in cathode air flow is the controlling mode of heat transfer. Conductive heat transfer also plays an important role; according to the modeling results presented in chapter 3, conduction makes approximately 10% of the total heat transfer. As a result, bipolar plate thermal conductivity and air velocity are among the key parameters that influence the stack temperature distribution.

The results of varying the air velocity and bipolar plate thermal conductivity are plotted in Figure 4-1 and Figure 4-2 respectively. By increasing the inlet air velocity, the maximum temperature drops considerably, as expected. Increasing the bipolar plate thermal conductivity also has a positive impact on reducing the temperature in the entire domain. Notice that the range of studied air velocity is a practical range of the operating

condition. Also the thermal conductivity of graphite bipolar plate has a wide range from 15 W/m.K to 400 W/m.K.

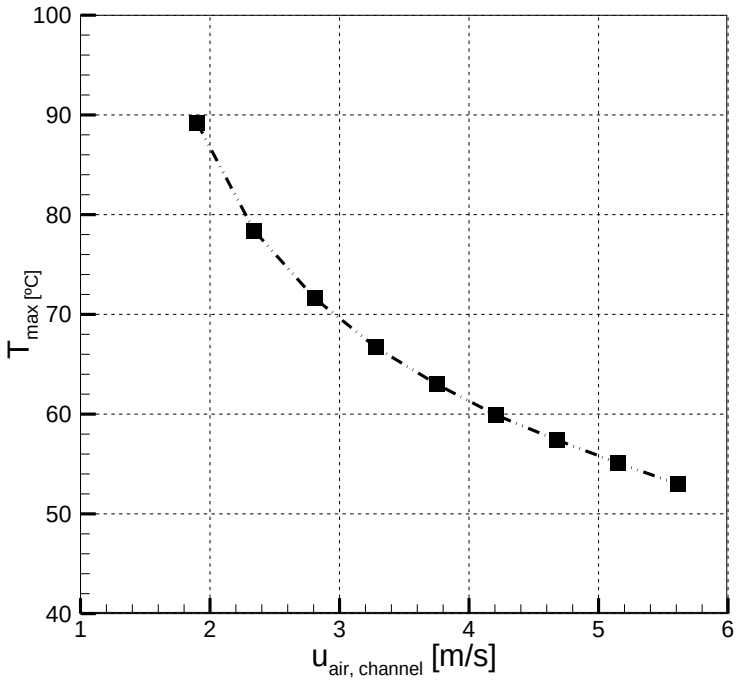

Figure 4-1: Effect of inlet air velocity on maximum temperature.

In Figure 4-3, the effect of the GDL thermal conductivity is investigated. It can be observed that unlike the bipolar plate thermal conductivity, which has significant impact on the temperature distribution, changing the GDL thermal conductivity does not change the results, at least within the studied range.

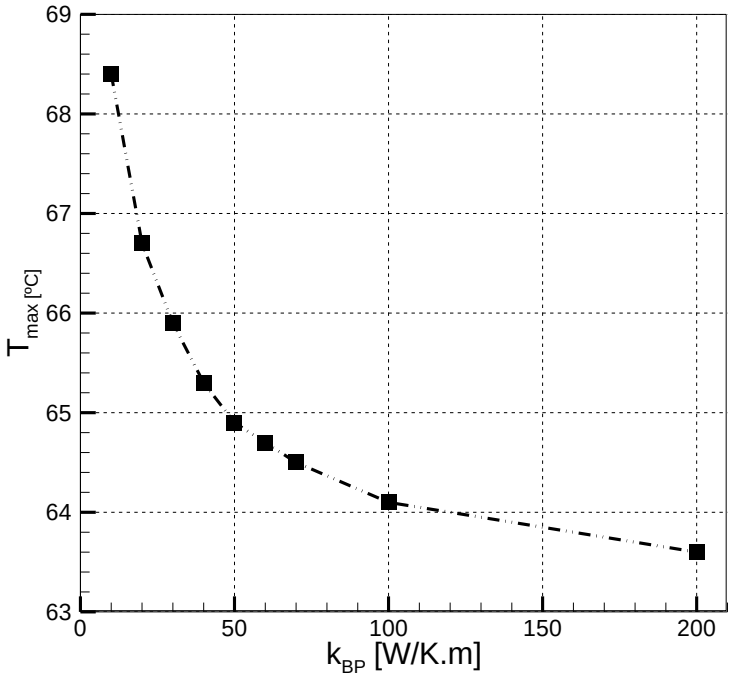

Figure 4-2: Effect of bipolar plate thermal conductivity on maximum temperature.

Moreover, the effect of anisotropic GDL thermal conductivity is studied in

Figure **4-4**. In one case, the in-plane and through plane thermal conductivities are 17 and 0.5 W/m.K respectively while in the other case isotropic GDL was considered with thermal conductivity of 0.5 W/m.K.

Similarly, the effect of isotropic and anisotropic bipolar plate thermal conductivity is investigated and temperature distributions are plotted in Figure 4-5 for comparison. This Figure shows that the impact of in-plane thermal conductivity of bipolar plate on the temperature distribution is more significant than the effect of through-plane thermal conductivity. As Figure 4-6 shows, higher thermal conductivity for bipolar plate leads to a more uniform temperature distribution.

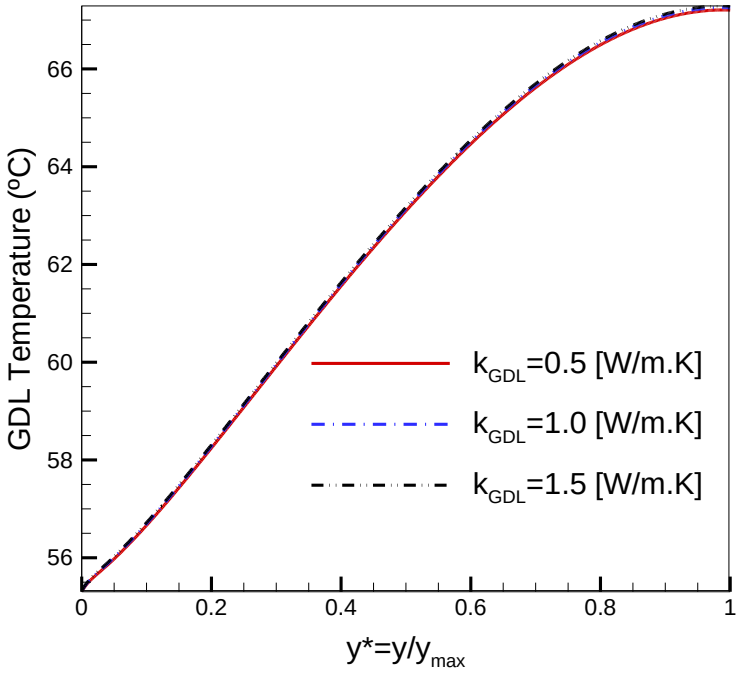

Figure 4-3: Effect of GDL thermal conductivity on GDL temperature distribution along the channel;

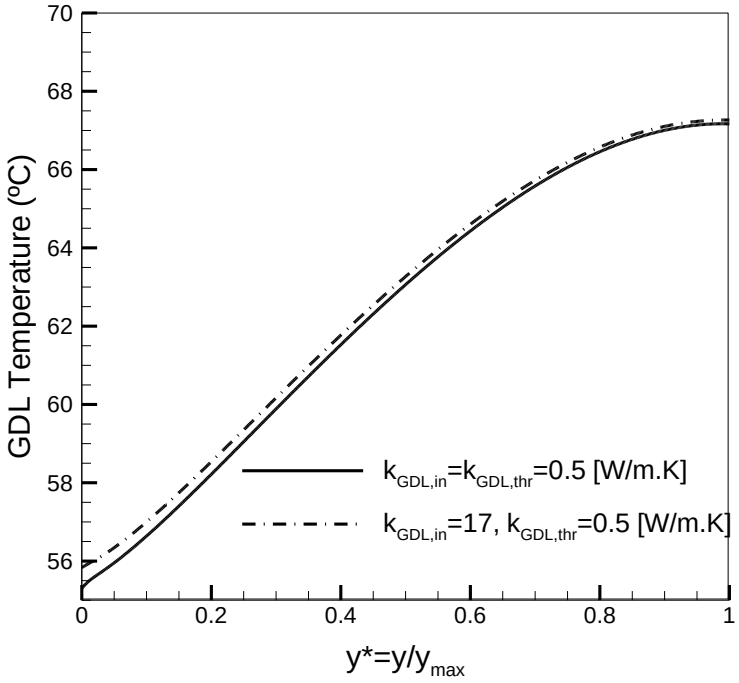

Figure 4-4: Effect of anisotropic GDL thermal conductivity on GDL temperature distribution along the channel.

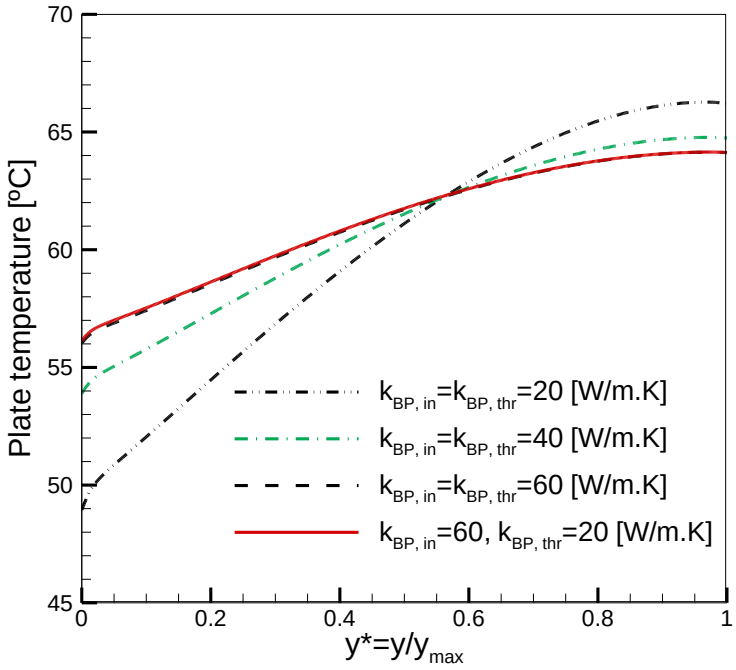

Figure 4-5: Different impact of in-plane and through-plane bipolar plate thermal conductivity on temperature distribution along the channel.

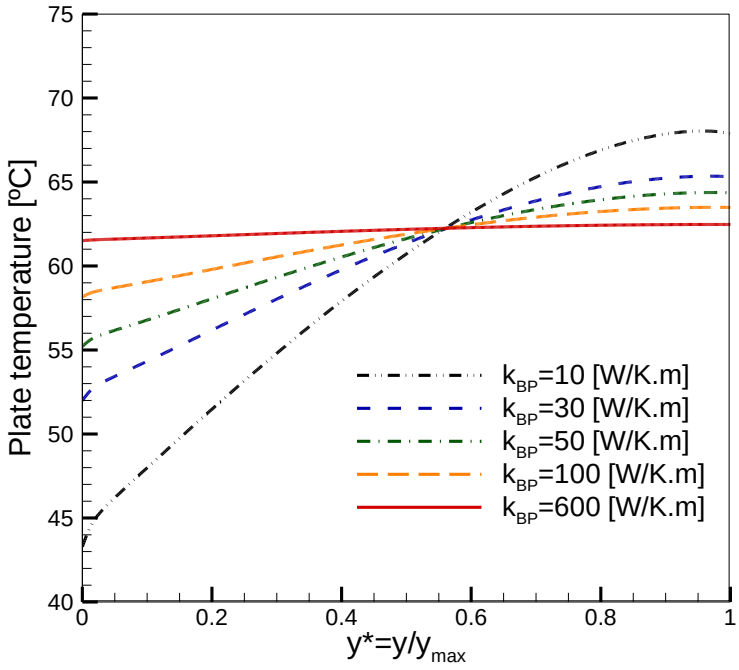

Figure 4-6: Effect of bipolar plate in-plane thermal conductivity on temperature distribution along the channel.

In the studied cases, the thermal contact resistance (TCR) between GDLs and bipolar plate was neglected. In this section, we have studied the effect of including TCR in our model.

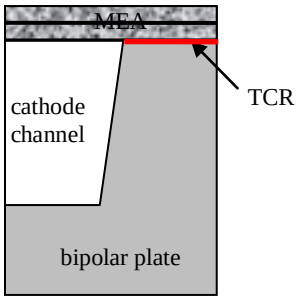

Figure 4-7: Schematic of the fuel cell channel model including thermal contact resistance (TCR)

As shown in Figure 4-7, we have considered a thin layer of a hypothetical material between bipolar plate and GDL, with an equivalent thermal conductivity to compensate for the effect of thermal contact resistance. The thickness of this layer, t_{eq}, is assumed be on the order of the GDL surface roughness (~ 10 μm). Due to computational limits, the smallest thickness that we could include in our model was 50 μm. However, we have verified that thinner layers have less effect on the results. This thermal conductivity is calculated by using the experimental data reported by Sadeghi et al. [38]. We have picked the maximum value of TCR and calculated the equivalent thermal conductivity, k_{eq}, using the following relation (k_{eq} =0.08 [W/m. K]):

$$k_{\mathrm{eq}} = \frac{t_{\mathrm{eq}}}{\mathrm{TCR}} \qquad \textbf{(4-1)}$$

The results of GDL temperature distribution along the channel are plotted in Figure 4-8 for a case neglecting TCR and the same case including TCR. As it can be seen in this figure, including TCR results in a slightly higher temperature distribution but the impact is negligible. This is a direct result of the convective-dominant heat transfer in the channel. In other words, the TCR will only affect the conduction heat transfer from GDL to bipolar plate, which is much smaller that the convection heat transfer from GDL to the air flow.

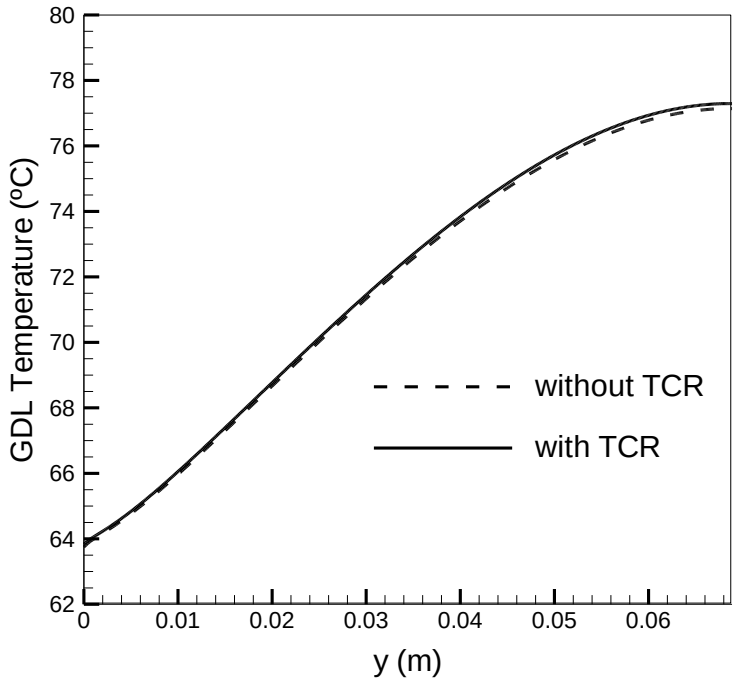

Figure 4-8: Effect of TCR on temperature distribution along the channel

4.2 Channel Geometry

To investigate the effect of channel geometry, all other parameters should be kept constant. Therefore, in addition to the constraint of constant channel cross-sectional area, constant cell area has to be considered. This means that the bipolar plate rib thickness

should vary accordingly with the variation of channel geometry. Figure 4-9 compares the temperature distribution in different channel geometries, i.e., trapezoidal, square, and rectangular cross-sections. This figure shows that under the conditions of constant oxidant flow rate and cross-sectional surface area, the plate temperature in rectangular channel is lower than that of trapezoidal channel. Also under the same conditions, in a trapezoidal channel bipolar plate has a lower temperature than in a square channel. This is caused by the contact surface area between air stream and GDL. A rectangular cross-section with aspect ratio of 0.5 in which the longer side is the top wall (GDL), provides a larger contact area between air and GDL compared to a square or a trapezoidal cross-section and therefore, enhances heat transfer. Similarly, in a trapezoidal channel, air has a larger contact surface with GDL and more heat can be rejected by forced convection.

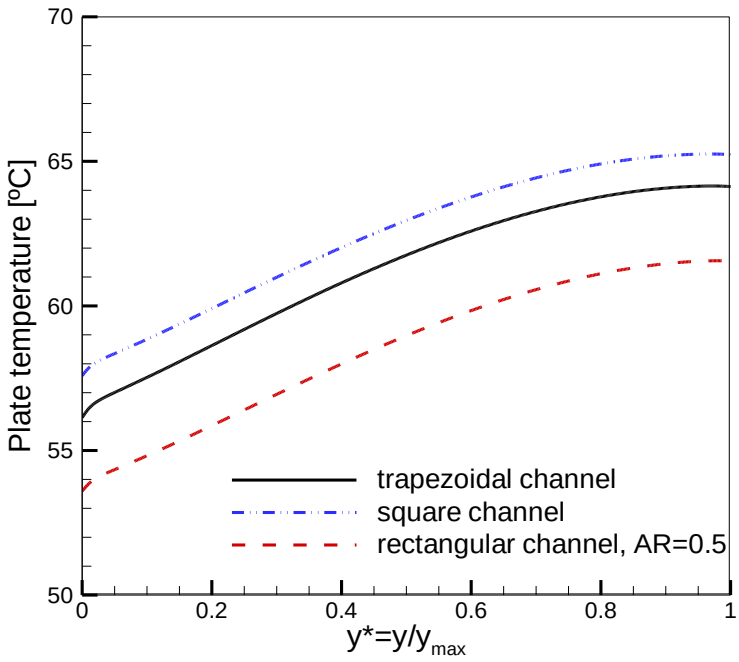

Figure 4-9: Temperature variation in flow direction for trapezoidal, square, and rectangular channel cross-sections.

The channel geometry not only affects the temperature distribution, but also changes the pressure drop. The oxidant relative pressure is plotted in Figure 4-10, which shows that trapezoidal channel has the lowest pressure drop among the considered geometries.

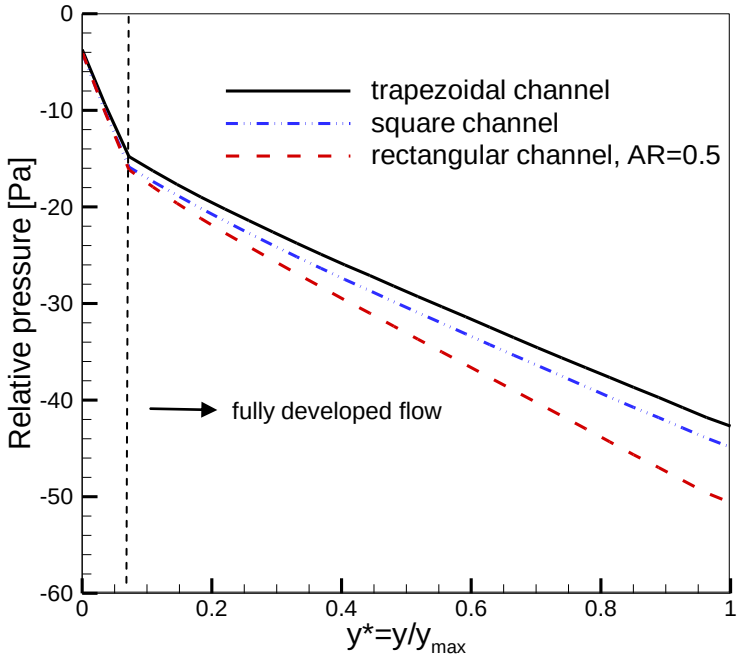

Figure 4-10: Oxidant relative pressure in flow direction for trapezoidal, square, and rectangular channel cross-sections.

The change in the trend of pressure drop in Figure 4-10 is due to the transition from hydrodynamically developing flow to fully developed flow.

5: CONCLUSIONS AND RECOMMENDATIONS

In order to develop techniques and strategies for cooling and thermal management of PEMFCs, numerical modeling is a strong method that has been much considered in recent years. In the present work, a three-dimensional thermal model is developed to predict the temperature distribution in a PEMFC. The proposed model can be used for design and optimization of cooling devices for PEMFC systems. This model provides the maximum temperature in an air-cooled PEMFC stack, without considering the whole stack as the solution domain.

The results show that in a single channel the bipolar plate temperature gradient is much higher in the flow direction than other directions. However, the oxidant temperature variation is considerable in all directions, which reveals the necessity of three-dimensional modeling.

Moreover, different heat transfer regimes are analyzed, which clearly shows that in air-cooled fuel cell stacks, where the air stoichiometry is high, the most significant heat transfer mode is the forced convective heat transfer. In fact, parametric studies show that the air velocity and bipolar plate in-plane thermal conductivity are among the critical factors that affect the temperature distribution in a PEMFC and thus play important roles in thermal management of PEMFCs. Bipolar plates can also function as heat spreaders. Therefore, it is recommended that highly thermal conductive materials such as pyrolytic graphite sheet (with thermal conductivity of 600 to 800Wm^{-1} K^{-1} in the in-plane

directions) be used in the stack [30]. Pyrolytic graphite sheet is highly thermal conductive, lightweight, flexible and heat-resistant, and has been applied successfully in the thermal management of commercial portable electrical devices like laptop computers, where the spaces are limited [39].

The validity of the numerical model is verified by comparison of the results with experimental data provided by Ballard Power Systems. The numerical and experimental values for the maximum temperature in the central channel are compared, which shows a good agreement. In most of the cases, our model slightly overestimates the maximum temperature. The main reason can be due to the assumptions that we made to determine the boundary conditions; we assumed that the central channel in the stack is insulated and there is no heat transfer to the adjacent channels. The other source of error can be uncertainty in thermophysical properties and input parameters such as air velocity and heat generation.

In our study, the GDL thermal conductivity does not change the temperature profiles significantly, although the results of some other studies in the literature such as [20] show that the GDL thermal conductivity strongly impacts the membrane temperature rise. This conflict rises from different mechanisms of heat transfer in air-cooled fuel cells and other types of fuel cells. In the studies that temperature distribution is sensitive to GDL thermal conductivity, the air stoichiometry is low (~2); however, in air-cooled fuel cells, the air stoichiometry is much higher (~100). Because of this high stoichiometry, the heat transfer in air-cooled fuel cells is primarily controlled by convection and thus GDL thermal conductivity does not play a major role. This conclusion is specific to the fuel

cell stacks in which convective heat transfer is considerably higher than conductive heat transfer.

We have also investigated the effect of channel geometry on temperature distribution and pressure drop. Channels with trapezoid, square, and rectangular cross-sections with equal surface area were compared in terms of temperature distribution and pressure drop. The results show that the trapezoidal channel gives the minimum pressure drop among the considered geometries while the rectangular channel gives the minimum temperature. Therefore, the selection of channel geometry remains to a trade off design analysis of operating temperature and pressure that can be considered as a future work.

For the future work, it is also possible to integrate the present thermal model with a performance model in order to investigate the effects of parameters, such as relative humidity, that influence the fuel cell current and voltage and finally change the amount of heat generation in the stack. This three-dimensional model for single cells can form a theoretical foundation for thermal analysis of multi-cell stacks where thermal management and stack cooling is a significant engineering challenge.

6: REFERENCE LIST

1. Larminie J, Dicks A (2003) Fuel Cell Systems Explained (2nd Edition) John Wiley & Sons
2. Faghri A, Guo Z (2005) Challenges and opportunities of thermal management issues related to fuel cell technology and modeling. International Journal of Heat and Mass Transfer 48: 3891-3920
3. Gasteiger HA, Mathias MF (2004) Fundamental research and development challenges in polymer electrolyte fuel cell technology. The third international symposium on proton conducting membrane fuel cells: 1-24
4. Endoh E, Terazono S, Widjaja H, Takimoto Y (2004) Degradation Study of MEA for PEMFCs under Low Humidity Conditions. Electrochemical and Solid-State Letters 7: A209-A211
5. van den Oosterkamp PF (2006) Critical issues in heat transfer for fuel cell systems. Energy Conversion and Management 47: 3552-3561
6. Xue X, Tang J, Smirnova A, England R, Sammes N (2004) System level lumped-parameter dynamic modeling of PEM fuel cell. Journal of Power Sources 133: 188-204
7. Yu S, Jung D (2010) A study of operation strategy of cooling module with dynamic fuel cell system model for transportation application. Renewable Energy 35: 2525-2532
8. Bao C, Ouyang M, Yi B (2006) Analysis of the water and thermal management in proton exchange membrane fuel cell systems. International Journal of Hydrogen Energy 31: 1040-1057
9. Yu X, Zhou B, Sobiesiak A (2005) Water and thermal management for Ballard PEM fuel cell stack. Journal of Power Sources 147: 184-195
10. Colella WG (2003) Modelling results for the thermal management sub-system of a combined heat and power (CHP) fuel cell system (FCS). Journal of Power Sources 118: 129-149
11. Linnhoff B, Senior PR (1983) Energy Targets Clarify Scope for Better Heat Integration. Process Engineering: 29-33
12. Chupin S, Colinart T, Didierjean S, Dubé Y, Agbossou K, Maranzana G, Lottin O (2010) Numerical investigation of the impact of gas and cooling flow configurations on current and water distributions in a polymer membrane fuel cell through a pseudo-two-dimensional diphasic model. Journal of Power Sources 195: 5213-5227

13. Shan Y, Choe S-Y (2005) A high dynamic PEM fuel cell model with temperature effects. Journal of Power Sources 145: 30-39

14. Siegel C (2008) Review of computational heat and mass transfer modeling in polymer-electrolyte-membrane (PEM) fuel cells. Energy 33: 1331-1352

15. Yu S, Jung D (2008) Thermal management strategy for a proton exchange membrane fuel cell system with a large active cell area. Renewable Energy 33: 2540-2548

16. Pharoah JG, Burheim OS (2010) On the temperature distribution in polymer electrolyte fuel cells. Journal of Power Sources 195: 5235-5245

17. Shimpalee S, Dutta S (2000) Numerical prediction of temperature distribution in PEM fuel cells. Numerical Heat Transfer Part A 38: 111-128

18. Adzakpa KP, Ramousse J, Dubé Y, Akremi H, Agbossou K, Dostie M, Poulin A, Fournier M (2008) Transient air cooling thermal modeling of a PEM fuel cell. Journal of Power Sources 179: 164-176

19. Sinha PK, Wang C-Y, Beuscher U (2007) Transport Phenomena in Elevated Temperature PEM Fuel Cells. Journal of The Electrochemical Society 154: B106-B116

20. Ju H, Meng H, Wang C-Y (2005) A single-phase, non-isothermal model for PEM fuel cells. International Journal of Heat and Mass Transfer 48: 1303-1315

21. Faghri A, Guo Z (2008) Integration of Heat Pipe into Fuel Cell Technology. Heat Transfer Engineering 29: 232-238

22. Sasmito AP, Lum KW, Birgersson E, Mujumdar AS (2010) Computational study of forced air-convection in open-cathode polymer electrolyte fuel cell stacks. Journal of Power Sources 195: 5550-5563

23. Spitta C, Mathiak J, Dokupil M, Heinzel A (2007) Coupling of a Small Scale Hydrogen Generator and a PEM Fuel Cell WILEY-VCH Verlag, pp. 197-203.

24. Scholta J, Messerschmidt M, Jörissen L, Hartnig C (2009) Externally cooled high temperature polymer electrolyte membrane fuel cell stack. Journal of Power Sources 190: 83-85

25. Asghari S, Akhgar H, Imani BF (2011) Design of thermal management subsystem for a 5 kW polymer electrolyte membrane fuel cell system. Journal of Power Sources 196: 3141-3148

26. Baek SM, Yu SH, Nam JH, Kim C-J (2011) A numerical study on uniform cooling of large-scale PEMFCs with different coolant flow field designs. Applied Thermal Engineering 31: 1427-1434

27. Kurnia JC, Sasmito AP, Mujumdar AS (2011) Numerical investigation of laminar heat transfer performance of various cooling channel designs. Applied Thermal Engineering 31: 1293-1304

28. Song T-W, Choi K-H, Kim J-R, Yi JS (2011) Pumpless thermal management of water-cooled high-temperature proton exchange membrane fuel cells. Journal of Power Sources 196: 4671-4679

29. Park YH, Caton JA (2008) Development of a PEM stack and performance analysis including the effects of water content in the membrane and cooling method. Journal of Power Sources 179: 584-591

30. Wen C-Y, Lin Y-S, Lu C-H (2009) Performance of a proton exchange membrane fuel cell stack with thermally conductive pyrolytic graphite sheets for thermal management. Journal of Power Sources 189: 1100-1105

31. Wen C-Y, Lin Y-S, Lu C-H, Luo T-W (2011) Thermal management of a proton exchange membrane fuel cell stack with pyrolytic graphite sheets and fans combined. International Journal of Hydrogen Energy 36: 6082-6089

32. Djilali N (2007) Computational modelling of polymer electrolyte membrane (PEM) fuel cells: Challenges and opportunities. Energy 32: 269-280

33. Gidaspow D (1969) Handbook of fuel cell technology, Carl Berger, Editor, Prentice-Hall, Englewood Cliffs, N. J. (1968). 607 pages. $18.50. AIChE Journal 15: 3-3 DOI 10.1002/aic.690150103

34. Incropera FP, Dewitt DP (1996) Fundamentals of Heat and Mass Transfer, fourth edn John Wiley & Sons., Inc., New York

35. Bolz R, Tuve G (1976) Handbook of tables for applied engineering science, 2nd edn CRC Press, Cleveland

36. Shahsavari S, Kjeang E, Bahrami M (2010) Analytical velocity and temperature distributions for flow in microchannels of various cross-sectionsThe 8th International ASME Conference on Nanochannels, Microchannels, and Minichannels, Monreal, Canada.

37. Shah RK, London AL (1978) Laminar flow forced convection in ducts : a source book for compact heat exchanger analytical data Academic Press, New York

38. Sadeghi E, Djilali N, Bahrami M (2011) Effective thermal conductivity and thermal contact resistance of gas diffusion layers in proton exchange membrane fuel cells. Part 1: Effect of compressive load. Journal of Power Sources 196: 246-254

39. http://panasonic.com/industrial/electronic-components/ (2010).